

The ESO supernovae type Ia progenitor survey (SPY)^{★,★★}

The radial velocities of 643 DA white dwarfs

R. Napiwotzki^{1,2}, C. A. Karl², T. Lisker^{2,3}, S. Catalán⁴, H. Drechsel², U. Heber², D. Homeier⁵, D. Koester⁶, B. Leibundgut⁷, T. R. Marsh⁴, S. Moehler⁷, G. Nelemans⁸, D. Reimers⁹, A. Renzini¹⁰, A. Ströer², and L. Yungelson¹¹

¹ Centre for Astrophysics Research, University of Hertfordshire, Hatfield AL10 9AB, UK
e-mail: r.napiwotzki@herts.ac.uk

² Dr. Remeis-Sternwarte & ECAP, Universität Erlangen-Nürnberg, Sternwartstr. 7, 96049 Bamberg, Germany

³ Astronomisches Rechen-Institut, Zentrum für Astronomie der Universität Heidelberg, Mönchhofstr. 12-14, 69120 Heidelberg, Germany

⁴ Department of Physics, University of Warwick, Coventry CV4 7AL, UK

⁵ Georg-August-Universität, Institut für Astrophysik, Friedrich-Hund-Platz 1, 37077 Göttingen, Germany

⁶ Institut für Theoretische Physik und Astrophysik, Universität Kiel, 24098 Kiel, Germany

⁷ European Southern Observatory, Karl-Schwarzschild-Str. 2, 85748 Garching, Germany

⁸ Institute for Astronomy, KU Leuven, Celestijnenlaan 200D, 3001 Leuven, Belgium

⁹ Hamburger Sternwarte, Gojenbergsweg 112, 21029 Hamburg, Germany

¹⁰ INAF – Osservatorio Astronomico di Padova, vicolo dell’Osservatorio 5, 35122 Padova, Italy

¹¹ Institute of Astronomy of the Russian Academy of Sciences, 48 Pyatnitskaya Str., 119017 Moscow, Russia

Received 4 September 2016 / Accepted 25 June 2019

ABSTRACT

Close double degenerate binaries are one of the favoured progenitor channels for type Ia supernovae, but it is unclear how many suitable systems there are in the Galaxy. We report results of a large radial velocity survey for double degenerate (DD) binaries using the UVES spectrograph at the ESO VLT (ESO SN Ia Progenitor survey – SPY). Exposures taken at different epochs are checked for radial velocity shifts indicating close binary systems. We observed 689 targets classified as DA white dwarfs (displaying hydrogen-rich atmospheres), of which 46 were found to possess a cool companion. We measured radial velocities (RV) of the remaining 643 DA white dwarfs. We managed to secure observations at two or more epochs for 625 targets, supplemented by eleven objects meeting our selection criteria from literature. The data reduction and analysis methods applied to the survey data are described in detail. The sample contains 39 double degenerate binaries, only four of which were previously known. Twenty are double-lined systems, in which features from both components are visible, the other 19 are single-lined binaries. We provide absolute RVs transformed to the heliocentric system suitable for kinematic studies. Our sample is large enough to sub-divide by mass: 16 out of 44 low mass targets ($\leq 0.45 M_{\odot}$) are detected as DDs, while just 23 of the remaining 567 targets with multiple spectra and mass $> 0.45 M_{\odot}$ are double. The detected fraction amongst the low mass objects ($36.4 \pm 7.3\%$) is significantly higher than for the higher-mass, carbon-oxygen core dominated part of the sample ($3.9 \pm 0.8\%$), but it is much lower than expected from the detection efficiency for companion masses of $0.05 M_{\odot}$ or higher and a 100% binary fraction. This suggests either companion stars of with a mass below $0.05 M_{\odot}$ or some of the low mass white dwarfs are single.

Key words. techniques: radial velocities – binaries: close – binaries: spectroscopic – supernovae: general – white dwarfs

1. Introduction

Type Ia supernovae (SNe Ia) play an important role in the study of cosmic evolution. For instance, they served as standardizable candles in the studies that led to the discovery of the acceleration of the Universe’s expansion (e.g. [Riess et al. 1998](#); [Perlmutter et al. 1999](#)). There is general consensus that SNe Ia events are the result of thermonuclear explosions in degenerate matter ([Hoyle & Fowler 1960](#)). However, the nature of their progenitors, explo-

sion mechanisms and the origin of different subclasses still pose serious problems.

Hoyle & Fowler suggested that explosion occurs when a critical mass (likely the Chandrasekhar limit, $1.4 M_{\odot}$) is reached. The most natural candidates for explosions are then white dwarfs (WDs) in binaries accreting matter from non-degenerate hydrogen companions via stable Roche-lobe overflow ([Schatzman et al. 1963](#); [Wheeler & Hansen 1971](#); [Whelan & Iben 1973](#)) or stellar wind capture ([Truran & Cameron 1971](#); [Tutukov & Yungelson 1976](#)). This is the earliest so-called “classical” single-degenerate (SD) scenario.

Another classical scenario is the double-degenerate (DD) one, in which explosion is, hypothetically, the outcome of the merger of two white dwarfs of (super)-Chandrasekhar total mass ([Webbink et al. 1979](#); [Tutukov & Yungelson 1979, 1981](#); [Webbink 1984](#); [Iben & Tutukov 1984](#)). The merger of components is

* Full Tables B.1 and C.2, final white dwarf spectra, and data for Fig. 3 are only available at the CDS via anonymous ftp to [cvsarc.u-strasbg.fr](mailto:cdsarc.u-strasbg.fr) (130.79.128.5) or via <http://cdsarc.u-strasbg.fr/viz-bin/cat/J/A+A/638/A131>

** Based on data obtained at the Paranal Observatory of the European Southern Observatory for programmes No. 165.H-0588, 167.D-0407, 71.D-0383, 72.D-0487.

caused by the orbital shrinkage due the loss of angular momentum via gravitational wave radiation and subsequent unstable mass loss. Initially, it was envisioned that the lighter of the two fills its Roche lobe first since $R_{\text{WD}} \propto M_{\text{WD}}^{-1/3}$. In systems with mass ratios $\geq 2/3$ the $M - R$ relation causes the merger to occur on the dynamical time scale (comparable to few orbital periods). The disrupted white dwarf transforms into a “heavy disc” or “envelope” from which the matter accretes onto the central object. This inference was confirmed by smooth particle hydrodynamics (SPH) calculations by [Benz et al. \(1990\)](#) and in many other theoretical studies.

It was later realised that the stability of the mass transfer also depends on the efficiency of spin-orbit coupling, which affects the variation of the accretion rate as the merger takes place ([Marsh et al. 2004](#)). SPH-calculations, using a physical equation of state, showed that the lighter component disrupts within about 100 orbital periods and the merger may proceed either via a disk or direct impact, depending on the mass ratio of the components ([D’Souza et al. 2006](#); [Dan et al. 2009](#)).

Currently, two possible DD scenarios are commonly discussed. In “violent” (a.k.a. “prompt”) mergers the matter of the lighter WD may, even before its complete disruption, start to accrete onto the surface of the companion on a dynamical timescale. Detonation is supposed to be initiated in a He+C+O mixture at the interface of the merging white dwarfs. Helium detonation produces a shock wave, which propagates and focusses towards the centre of the accretor and results in ignition of carbon and explosion ([Livne 1990](#); [Livne & Glasner 1991](#)).

If the explosion does not occur promptly at lower mass ratios than required for violent merger, (see, e.g., discussion by [Sato et al. 2016](#)), an object consisting of a cold virtually isothermal core, a pressure-supported envelope, a Keplerian disc, and a tidal tail forms ([Guerrero et al. 2004](#)). A He or C+O-mixture may explode in the envelope which is the hottest part of the object and lead to the detonation of carbon at the periphery of the accretor. If two C/O white dwarfs merge together gradually, the outcome depends on the rate of settling of the envelope matter onto the core. Either the central ignition of carbon and SN Ia occurs, or a neutron star or a massive oxygen-neon (O/Ne) white dwarf forms ([Nomoto & Iben 1985](#); [Mochkovitch & Livio 1990](#)).

In both of the DD scenarios, explosion of the C/O core, which may have a sub-Chandrasekhar mass, results in the disruption of the entire configuration. The major fraction of the accretor mass burns to radioactive Ni. This determines the optical luminosity and the spectrum of the SN. The donor burns to intermediate mass elements, which define the observational manifestations of SNe at maximum brightness ([Shigeyama et al. 1992](#); [Sim et al. 2010](#)).

An advantage of the DD scenario is that it produces a delay-time distribution (DTD) which overlaps with the Hubble time. The delays are shorter than ≈ 3 Gyr (see, e.g. [Yungelson 2010](#); [Bours et al. 2013](#)) for the SD channel. If all types of mergers are taken into account, C/O core pairs (C/O+C/O), as well as mergers of C/O white dwarf and massive He and hybrid (C/O core + thick He mantle) white dwarfs, then population synthesis studies can reasonably reproduce the current Galactic SNe Ia rate as well as the slope of their observationally inferred delay time distribution (e.g. [Yungelson & Kuranov 2017](#)). We refer the interested reader for further details concerning evolution of close binaries leading to the formation of progenitors of SNe Ia and the physical processes involved in explosions of SN Ia and their observational manifestations to a number of recent reviews (e.g. [Hillebrandt et al. 2013](#); [Postnov & Yungelson 2014](#); [Maoz et al. 2014](#); [Ruiz-Lapuente 2014](#); [Branch & Wheeler 2017](#);

[Taubenberger 2017](#); [Livio & Mazzali 2018](#); [Röpke & Sim 2018](#), and references therein).

The significance of the DD scenario relies upon the existence in nature of a sufficient number of DDs prone to merge and the physical parameters of their components. A given Galactic SN Ia rate and pre-supernova lifetime implies a specific number of progenitors in the Galaxy. Searches for DDs thus test them as progenitors of type Ia SNe, but also provide benchmarks for testing the theory of binary star evolution, since in the process of formation, DDs pass through two to four very badly understood stages of common envelope evolution.

The first known DD, L870–2, was discovered by chance in the 1980s ([Saffer et al. 1988](#)), but its orbital period of 1.55 days is too long for it to merge within a Hubble time and thus be representative of the putative DD progenitors of present-day type Ia supernovae, which must have periods of less than ten to 15 h. Systematic surveys of the same decade ([Robinson & Shafter 1987](#); [Foss et al. 1991](#)) failed to find any DDs among 44 and 25 targets, respectively. A sure-fire DD as well as some candidates were found by [Bragaglia et al. \(1990\)](#) among 54 objects. The (premature) conclusion of these studies was that the space density of DDs was below that required for reproducing the observed rate of SNe Ia. The low masses ($M_{\text{tot}} < M_{\text{Ch}}$) of the confirmed and candidate DDs as well as their long merger timescales were raised as further arguments against the DD scenario.

In the 1990s, more successful targeted searches were made, focusing upon low mass (helium) white dwarfs, which primarily form via binary evolution ([Marsh 1995](#); [Marsh et al. 1995](#); [Moran et al. 1997](#); [Maxted et al. 2000a](#)). By the year 2000, around 180 white dwarfs had been checked for RV variations yielding a sample of 18 DDs with $P < 6\%$ ([Marsh 2000](#); [Maxted et al. 2000b](#)). None of the 18 discovered DD systems seemed massive enough to qualify as a SN Ia precursor. However, by this time, theoretical simulations suggested that less than a percent of all potentially observed white dwarfs are close DDs qualifying as SN Ia progenitors ([Iben et al. 1997](#); [Nelemans et al. 2001a](#)), and so the failure to find a clear progenitor in 180 white dwarfs is not a surprise.

The observational focus of the 1990s on low mass white dwarfs as more promising targets for DDs worked against the chances of finding potential type Ia progenitors. Still, given the ubiquity of white dwarfs, the number of DDs found showed that there is a large population of these binaries within the Galaxy. Clearly a definitive test of DDs as SNe type Ia progenitors requires (a) a larger sample of targets, and (b) one not selected by mass. We therefore embarked upon a large spectroscopic survey of white dwarfs using the UVES spectrograph at the ESO VLT UT2 (Kueyen) to search for white dwarfs and pre-white dwarfs with variable RVs (ESO SN Ia Progenitor survey – SPY). There have been a number of introductory articles to SPY ([Napiwotzki et al. 2003, 2001a, 2005](#)) and many results ([Napiwotzki et al. 2002, 2004, 2007](#); [Pauli et al. 2003](#); [Nelemans et al. 2005](#); [Koester et al. 2005a](#), to name a few), but there has been no full write-up of the original radial velocity survey. In this paper our aim is to accomplish this for the majority hydrogen-atmosphere DA white dwarfs.

Since the completion of the SPY survey, there have been many discoveries of DDs dominated by the light of “extremely low mass” (ELM) white dwarfs ([Brown et al. 2010, 2012, 2016a,b](#)), many of which will merge well within a Hubble time ([Kilic et al. 2012](#)). These discoveries post-date the SPY survey since ELM white dwarfs were missed in earlier surveys for white dwarfs due to their low gravities which makes them hard to distinguish from early-type main-sequence stars. Some of the

ELM binaries host massive white dwarfs hidden in the glare of the ELM components (Kulkarni & van Kerkwijk 2010; Marsh et al. 2011; Brown et al. 2013). If the mass ratio of components in ELM DDs allows stable mass exchange, they will turn into ultracompact cataclysmic variables of the AM CVn type (Faulkner et al. 1972; Nelemans et al. 2001b). In these systems, the accretors can in principle very occasionally reach the Chandrasekhar mass (Solheim et al. 2005). Otherwise, unstable mass transfer may lead to the merger of components with formation of subdwarf B, subdwarf O or R CrB stars; explosive events are not expected because of the small mass of the donors (Dan et al. 2014).

In this paper we present results of the SPY survey for the radial velocities of white dwarfs spectral type DA (hydrogen dominated spectra). The project was conceived for being operationally (and scientifically) advantageous with observations in service mode at the VLT that could be executed when the telescope would otherwise have been idle (Renzini 1999). Our sample overlaps strongly with the 615 SPY DAs analysed by Koester et al. (2009). Koester et al. performed a model atmosphere analysis of SPY spectra and determined the fundamental parameters effective temperature (T_{eff}) and surface gravity ($\log g$). Our focus is upon radial velocities, but we present additional fundamental parameter estimates to provide a uniform set of data for future comparison with theoretical models. The sample selection for SPY, observations, and data reduction are described in Sect. 2. Our method of RV measurement is outlined in Sect. 3. Section 4 presents the results including the detected DDs. In Sect. 5 we discuss our results in the context of previous surveys and implications for the evolution of DDs.

2. Observations and data analysis

2.1. Sample selection

Targets for SPY were drawn from five sources: the WD catalogue of McCook & Sion (1999), the Hamburg ESO Survey (HES; Wisotzki et al. 2000; Christlieb et al. 2001), the Hamburg Quasar Survey (HQS; Hagen et al. 1995; Homeier et al. 1998), the Montreal-Cambridge-Tololo survey (MCT; Lamontagne et al. 2000), and the Edinburgh-Cape survey (EC; Kilkenny et al. 1997). Our selection criteria were spectroscopic confirmation as a white dwarf (at least from objective prism spectra) and $B, V \leq 16.5$ (depending on what information was available) for the region south of $\delta = +15^\circ$. The limit was chosen in order to generate a sample size of order 1000 as thought necessary to uncover a potential SN Ia progenitor (DD with $M_{\text{tot}} \geq M_{\text{Ch}}$, Nelemans et al. 2001a). We extended the survey region later to include the region $+15^\circ \leq \delta \leq 25^\circ$, but imposed a brightness limit of $B, V \leq 15.5$.

The sample of white dwarfs catalogued by McCook & Sion (1999) incorporates various sets plagued with different selection effects. While early surveys for white dwarfs typically based their selection on proper motions (Luyten 1979; Giclas et al. 1978), later catalogues of white dwarfs are usually a waste-product of surveys for galaxies and quasars at high galactic latitude. One important early example is the Palomar-Green survey (Green et al. 1986) which used blue colour besides the galactic latitude as criterion. Similar approaches were used by the MCT and EC surveys mentioned above. Since photographic prism spectra are available for the HQS and HES surveys the presence of strong Balmer lines could be incorporated in the selection process (Christlieb et al. 2001) and the colour criterion could be somewhat relaxed. Other white dwarfs were identified because they showed up in EUV/X-ray surveys (e.g. Pounds et al. 1993). While these approaches have somewhat complementary selection

effects, there does remain a significant deficit of white dwarfs in the Galactic plane (Fig. 1). A small selection of our own was to avoid stars that satisfied our selection criteria but which had already been observed by Maxted et al. (2000b). Three of them ended up being re-observed during our survey, leaving an addition of seven to the SPY sample¹. We account for these stars later when discussing the detection efficiency of the SPY sample.

We had to create a large data base of accurate coordinates and finder charts at short notice to start the service mode observations for SPY. To speed up this process we initially focussed on catalogues with good coordinates and/or good finder charts. Important sources of the SPY observations reported in Koester et al. (2001, 2009) were the PG, HES, EC, and MCT surveys, which are all biased toward hot objects. Additional sources were the proper motion selected white dwarfs of Giclas et al. (1978, 1980) as catalogued in McCook & Sion (1999). Napiwotzki et al. (2005) reported on results from a “bright” sub-sample of SPY, which covers 93% of all known white dwarfs in the survey area. This sample should be virtually free of any SPY-related selection effects. In Fig. 1 we show the Aitoff projection in galactic coordinates of the DA white dwarfs observed by the SPY project. This figure shows the paucity of white dwarfs in the Galactic plane that we referred to above.

2.2. Observations

Spectra were taken with the UV-Visual Echelle Spectrograph (UVES) of the UT2 telescope (Kueyen) of the ESO VLT. UVES is a high resolution Echelle spectrograph, which can reach a resolution of 110 000 in the red region with a narrow slit (cf. Dekker et al. 2000, for a description of the instrument). Our instrument setup (Dichroic 1, central wavelengths 3900 Å and 5640 Å) uses UVES in a dichroic mode with a 2048 × 4096 EEV CCD windowed to 2048 × 3000 in the blue arm, and two CCDs, a 2048 × 4096 EEV and a 2048 × 4096 MIT-LL, in the red arm. Nearly complete spectral coverage from 3200 Å to 6650 Å with only two ≈ 80 Å wide gaps at 4580 Å and 5640 Å is achieved. In the standard setting used for our observations UVES is operated with an 8” decker in the blue arm and an 11” decker in the red arm. The slit was rotated to the parallactic angle.

SPY was implemented as a service mode programme. It took advantage of observing conditions which were not usable by most other programmes (moon, bad seeing, clouds), and was run when other programmes were not feasible. A wide slit (2”1) was used to minimise slit losses and a 2 × 2 binning applied to the CCDs to reduce read out noise. Our wide slit reduced the spectral resolution to $R = 18\,500$ (0.36 Å at H α) or better, if seeing disks were smaller than the slit width. Depending on the brightness of the objects, exposure times of 5 min or 10 min were chosen. The signal-to-noise ratio (S/N) per binned pixel (0.044, and 0.032 Å for the blue and red channel respectively) of the extracted spectrum is usually 15 or higher. Due to the nature of the project, two spectra at different, “random” epochs separated by at least one day were observed.

Although our programme was carried out during periods of less favourable observing conditions, the seeing was often smaller than the selected slit width of 2”1. This can, in principle, cause wavelength shifts, if the star is not placed in the centre of the slit. However, since according to the standard observing procedure the star was first centred on a narrow slit before the exposure with the broader slit was started, it can be expected

¹ WD 0401+250, WD 0752–146, WD 0950–572, WD 0954+247, WD 0954–710, WD 1407–475, WD 2151–015.

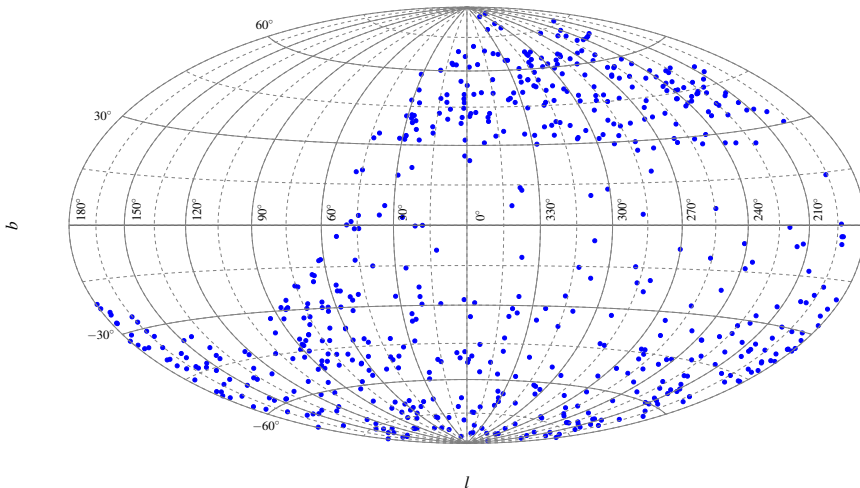


Fig. 1. Aitoff projection in Galactic coordinates of the DA white dwarfs observed by SPY.

that the star is usually relatively well centred in the slit. We used telluric lines present in the red region of some spectra to estimate the size of the resulting wavelength shifts (Sect. 2.4) and estimated an additional RV scatter of 0.67 km s^{-1} .

2.3. Data reduction

ESO provided at the time of the SPY observations (commencing in 2000) a data reduction pipeline for UVES, based on MIDAS procedures. The quality of the reduced spectra is in most cases good and we made extensive use of the pipeline reduced spectra for selecting targets for follow-up observations and the model atmosphere analysis of Koester et al. (2001). However, sometimes the reduction pipeline produced artefacts of varying strength, e.g. a quasi-periodic pattern in the red region similar in appearance to a fringing pattern. In a few cases either the blue or the red part of the pipeline reduced spectrum had extremely strong artefacts of unknown origin.

Therefore we created a semi-automatic “SPY pipeline” to perform the final reduction of the spectra. Our procedure makes use of several routines of the “UVES” context of MIDAS, which provides reduction routines adapted for the UVES spectrograph. The reduction is done individually for the blue (3200–4500 Å), lower red (4600–5600 Å), and upper red (5700–6650 Å) region of the spectrum. The position of the individual orders on the CCD is defined automatically tracing the order definition flatfield. However, usually the star is not perfectly centred on the slit along the spatial axis in all wavelength regions. The offset from the centre is determined and accounted for manually, along with the width of the stellar spectrum and the corresponding sky background area.

After accounting for cosmic ray hits and bad CCD pixels, bias and interorder background are subtracted. Wavelength calibration is then performed automatically using the Th-Ar reference spectrum. This is followed by the extraction of one dimensional spectra for each order of the sky background, flatfield, and object frames. For each spectrum, sky background subtraction and flatfielding are performed, and finally the orders are merged. Now, the resulting spectrum is divided by a smoothed spectrum of a DC WD, which by definition shows no spectral features at all and therefore provides an excellent means of correcting for the instrumental response. We checked a number of white dwarfs classified DC for the absence of spectral features even at our high resolution and selected two feature free ones (WD 0000–345 and WD 1520–340).

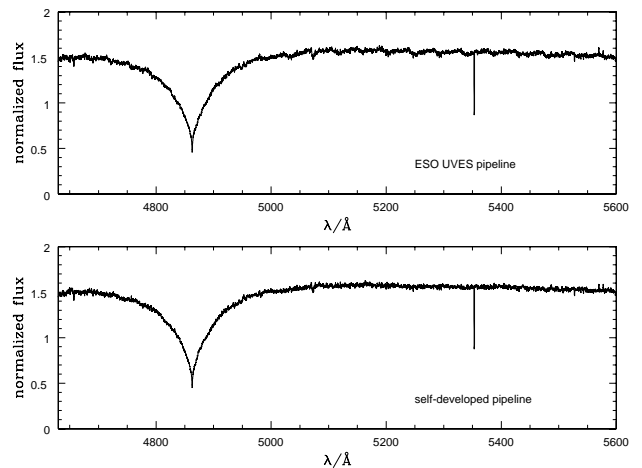


Fig. 2. Ripple problem and its solution. The *top spectrum* shows the reduced and merged spectrum of a DA WD. It displays a strong quasi-periodic pattern. The *lower spectrum* resulted after application of our “shift correction”.

A number of merged spectra did not appear smooth, but instead displayed a quasi-periodic ripple pattern over the whole wavelength range or at least over a significant part (Fig. 2). The appearance is similar to the effect mentioned above seen in some of the pipeline reduced spectra. Obviously, this behaviour is due to a mismatch in the flux levels of the corresponding ends of adjacent orders. Such effects should in principle be accounted for by the flatfield division. We do not find a relation as to when flatfield division is performed, since the ripples remain unchanged if we first divide the (two-dimensional) object and flatfield frames, and then extract the individual orders. In order to investigate this problem, we chose several stars where the signal-to-noise was large enough that we could extract each order with the width of only one pixel, and still obtain a useful resulting spectrum. The flatfield orders were extracted in the same way, but with an offset perpendicular to the dispersion direction (hereafter separation). We now went through a range of separations, and found that the ripples first disappear, then appear again with different shape. However, the separation which yields the smoothest spectrum is not always zero and the ideal separation changes with wavelength. To summarise, it is apparent that for each “pixel row” of the two dimensional object spectrum, there is only one flatfield pixel row which fits ideally, but this can change as one moves along the order.

Given that we do not understand the problem’s cause, it would seem unreasonable to construct a complex algorithm which would take these findings into account. However, without direct relation to the former, we found that the reduction can be improved significantly by shifting the flatfield orders with respect to the object orders a few pixels in the dispersion direction (as opposed to the perpendicular separation discussed above). This appears counterintuitive, but it produced the desired result and the practical implementation was easier.

The offset changed from night to night and sometimes between spectra taken the same night. This was taken into account in the reduction routine, which automatically went through a range of shift values. We selected spectral regions without strong features. For each shift, the reduced spectrum was fitted by a low-order polynomial, and χ^2 was computed from the difference between the spectrum and the fit. The best shift was chosen to be the one which led to the lowest χ^2 value. For each star, the shift was computed individually, although it was then applied to the flatfield, which is the same for all stars of one night. We emphasise that this does not correspond to a real wavelength shift of the spectra. This is demonstrated by our assessment of the stability of the wavelength scale in the Sect. 2.4.

The procedure outlined above works very well for the DAs (Fig. 2), which are the topic of this article, and for most other white dwarf spectral classes as well. However, for stars of other spectral types, e.g. helium-sdOs which show a large number of spectral lines, the automatic determination of the shift does not yield a useful result because the spectrum is too crowded with features. For these stars we determined the best shift manually by comparing the reduction results for various shifts. The determined shift values show no correlation with quantities like airmass or observing time. Although usually the overall shift varies only slightly during one night, there can be stars with completely different shift values, which do not stand out by position, observing time, or any other quantity. We therefore conclude that the observed effect must be intrinsic to the object frames, not to the flatfield which is only taken once per night. However, we could not identify an obvious reason for the origin of this problem.

We also included the observations from the later run 072.D-0487(A), taken during January, February and March 2004. This last set of data was reduced using the Reflex pipeline (Freudling et al. 2013). Reflex is an environment that was developed to provide an easy and flexible way to reduce VLT/VLTI science data using the ESO pipelines. The output data after using the pipeline are wavelength and flux calibrated spectra. The ripple problem occurs less often in the latest pipelines.

2.4. Telluric lines

A number of telluric absorption features are known in the red spectral range. In the $H\alpha$ region these are mostly caused by water in the atmosphere. Overall Paranal is a very dry place and thus the water features in our UVES spectra are usually weak. However, since the SPY spectra were taken preferentially during periods of relatively poor weather conditions, stronger telluric absorption is present in a number of spectra. Since the RV determination can be skewed if a strong telluric feature coincides with the stellar $H\alpha$ core, we corrected the telluric contribution.

For this purpose we produced a telluric UVES template, which was created from 50 UVES spectra selected from the complete SPY data set of ≈ 2000 spectra on the basis of strong water absorption and simple spectral appearance in the red range. This included white dwarfs of spectral types DA, DB, DBA, and DC. For each spectrum the local continuum was eval-

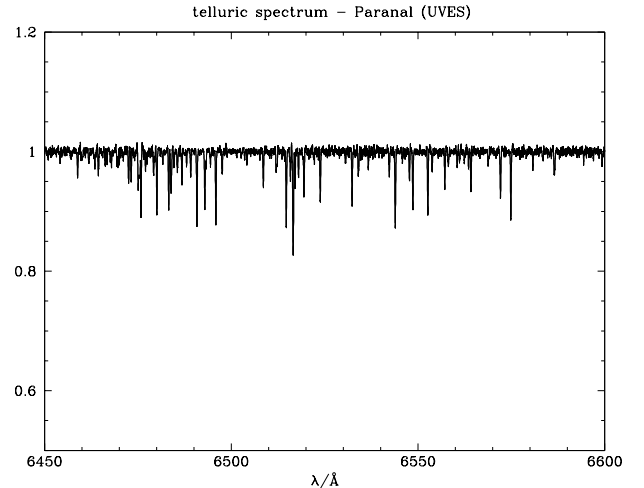


Fig. 3. Telluric template spectrum in the $H\alpha$ region.

uated in an iterative procedure. The spectra were convolved with a Gaussian of 1 \AA FWHM. Data points more than $3\times$ the noise level below the continuum were clipped. This procedure was repeated until the number of clipped wavelength points remained constant. The noise level was estimated from neighbouring featureless parts of the spectra. The inner line cores of $H\alpha$, if present, were excluded by hand. Since the white dwarf sample covers a large range of RVs, this does not produce gaps in the final co-added spectrum. Finally each spectrum was divided by the smoothed continuum. The individual spectra were rebinned to a common wavelength scale and the absorption was scaled to a “normalised telluric absorption strength”. Afterwards all 50 individual telluric spectra were co-added to the template spectrum shown in Fig. 3.

To correct the telluric contamination of the stellar spectra, we measured the strength of the telluric features in the 6450 \AA to 6500 \AA interval. No sharp stellar lines are present in this range. The template was scaled accordingly and the correction was done by dividing the stellar spectrum by the scaled template.

The presence of telluric lines complicates the analysis of the stellar spectra. However, there is a bright side as well. Telluric absorption lines can be used to measure RV velocities to very high precision (Griffin 1973). We checked the RV stability of the UVES/SPY observations by cross-correlating the template with individual spectra with strong telluric features. The resulting scatter is equivalent to $\pm 0.67 \text{ km s}^{-1}$ indicating good stability; this number was added in quadrature to the radial velocity uncertainties described in the next section when it came to judging evidence for radial velocity variability.

3. Radial velocity measurement

The radial velocities (RVs) of DA can be most accurately measured from the sharp line cores of the Balmer lines. These are most pronounced in $H\alpha$, and to an lesser extent in $H\beta$ (Fig. 4). These line cores are formed in high layers of the stellar atmosphere, where the density is low and pressure broadening small². The low densities allow the occupation numbers to deviate from

² Halenka et al. (2015) carried out theoretical calculations and claimed that pressure shift can mimic RV shifts of tenth of km s^{-1} , if the inner line wings of $H\beta$ are measured. The authors found negligible effects for $H\alpha$. Our empirical test presented in Appendix A indicates a much smaller effect, if present at all.

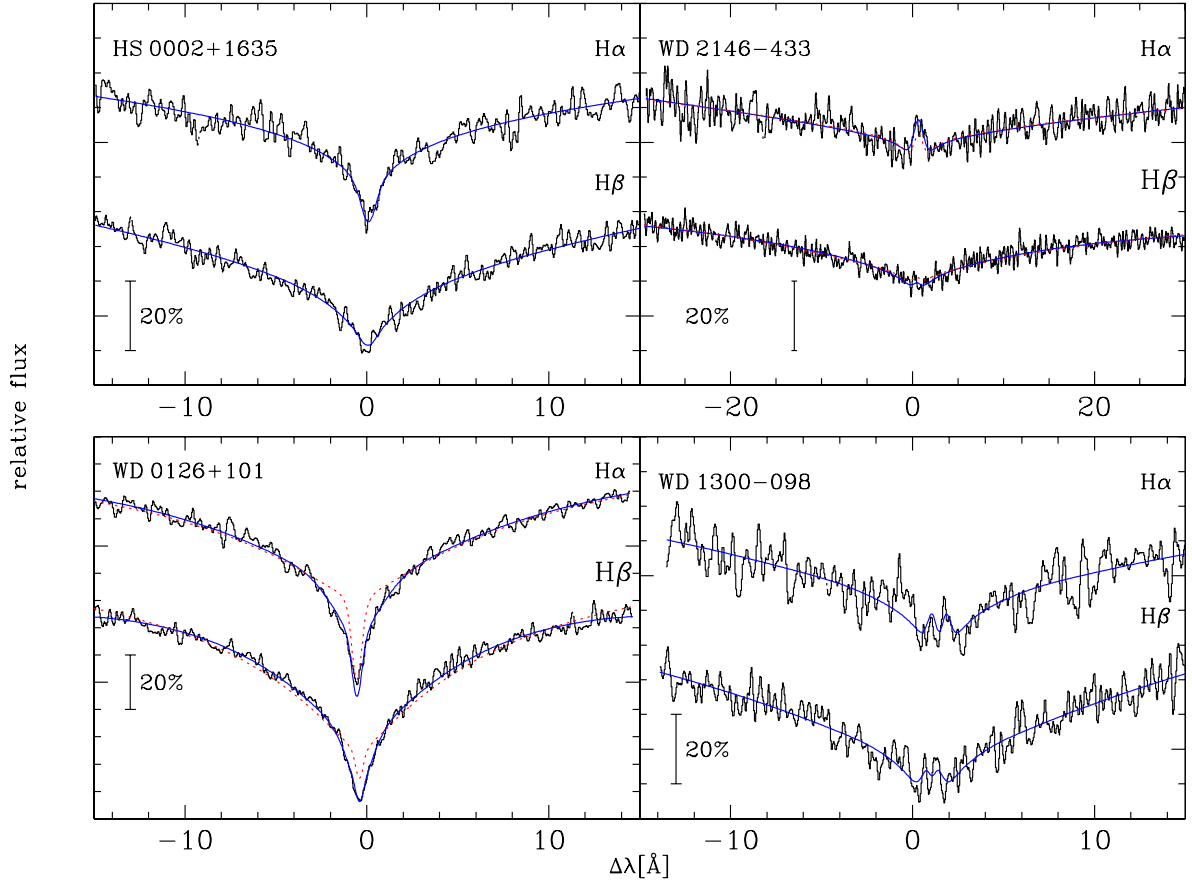


Fig. 4. Observed $H\alpha$ and $H\beta$ profiles compared to the fitted model spectrum. The graph shows one observed spectrum for each binary and the best fitting model spectrum (blue smooth line). Here and in the following figures we display the observed spectra smoothed with a Gaussian of 0.15 \AA FWHM, hardly affecting the spectral resolution. $\Delta\lambda$ is the wavelength offset relative to the laboratory wavelengths of $H\alpha$ and $H\beta$, respectively. *Top left:* HS 0002+1635, fitted with model spectra without modifications. *Top right:* WD 2146-433, a hot DA with a Gaussian added to better reproduce the central emission core (model spectrum without correction shown as dashed red line). *Bottom left:* WD 0126+101, one of the cool DAs displaying a broader and stronger central core than predicted by the models (model spectrum without correction shown as dashed red line). *Bottom right:* WD 1300-098, one of the magnetic white dwarfs.

local thermal equilibrium (LTE) and allow for NLTE effects, which are responsible for the strength of the cores (Greenstein & Peterson 1973). Since most white dwarfs are slow rotators (Koester & Herrero 1988; Heber et al. 1997a; Koester et al. 1998), the line cores are basically Gaussian with widths corresponding to the temperature in the formation layer.

Radial velocities of stars are often measured using cross-correlation algorithms. Observed spectra are correlated against model spectra or observed template spectra. The advantages of this method are the flexibility and its straightforward usage. As discussed in Napiwotzki et al. (2001a), the broad line wings of the Balmer lines cause complications if the traditional cross-correlation method is applied to white dwarfs. Thus we developed a modification of the cross-correlation method, which is based on a χ^2 test (Napiwotzki et al. 2001a) and measured the relative RV shifts between the observed spectra. This proved to be a quick and flexible way to select RV variable stars for follow-up observations (e.g. Napiwotzki et al. 2001b). However, experience showed that this method has its drawbacks (error estimates are not always reliable and sometimes spurious results are produced, especially for stars with weak line cores) and thus we developed more sophisticated methods for the final analysis. Another motivation for a different approach to the RV measurements was our interest to use the absolute RVs for a study of the

space velocities of the white dwarfs in the SPY sample (Pauli et al. 2003, 2006; Richter et al. 2007).

Several investigations (Saffer et al. 1988; Foss et al. 1991; Marsh et al. 1995; Maxted & Marsh 1999) modelled the line profiles with Lorentzians or Gaussians. However, these functions describe the line profiles only approximately and combinations of three or four functions can be necessary for an accurate modelling (Maxted & Marsh 1999). Model atmosphere line profiles on the other hand can reproduce the observed Balmer lines of DA white dwarfs quite accurately (Heber et al. 1997a), if the NLTE effects are taken into account. Koester et al. (2001) determined fundamental parameters of about 200 white dwarfs observed during the first nine months of the SPY observations, 163 of them of spectral type DA (compiled in their Table A.1). Koester et al. (2009) obtained the parameters of a much larger sample (including 615 DA white dwarfs). Thus, all the necessary information to apply line profile fits is available for our sample.

3.1. Model atmospheres

Radial velocities are derived by fitting the profiles of the $H\alpha$ and $H\beta$ Balmer lines with model spectra and computing the optimum RV. In the few cases with a clear detection of

photospheric Ca II H&K lines, these were also included. White dwarfs with temperatures above 20 000 K were analysed with the grid of self-consistent pure hydrogen NLTE model atmospheres for DA white dwarfs of Napiwotzki et al. (1999). Cooler white dwarfs were analysed with the grid described in Koester et al. (1998). These model spectra used NLTE line formation physics as applied to the LTE atmosphere models of Koester et al. (1994).

Fundamental parameters are derived from the spectral analysis of the complete Balmer series as described in Koester et al. (2009) for the SPY DA sample. The input physics of the model grids used for determining the RVs is not exactly the same as for the models used for the Koester et al. (2009) analysis. Thus we redetermined the fundamental parameters temperature and gravity with the grids actually used for the RV measurement and the fitting program FITSB2 described below. This ensures that the fitting process is self-consistent.

In the case of double-lined systems, temperatures and gravities of both components were determined. This was an iterative process with a first fit carried out using first guess RVs. The estimated fundamental parameters were then used for determining RVs from fitting the H α and H β lines. These initial estimates were refined by refitting temperature/gravity and RVs until parameter changes in subsequent steps became negligible. Model spectra for the two parameter sets were coadded after scaling them accordingly using the mass-radius relations derived from the tracks of Benvenuto & Althaus (1999) complemented by the Hamada & Salpeter (1961) zero temperature models for the highest masses. During these fits, the white dwarf mass-radius relation was used as a constraint to reduce parameter degeneracy.

3.2. FITSB2 and the fit process

The program FITSB2 can fit line profiles and measure RVs. It was originally developed to analyse the spectra of double-lined (SB2) systems, but can be applied to spectra of single-lined systems (RV variable or not) as well.

The basic philosophy for fitting line profiles follows the FITPROF program described in Napiwotzki et al. (1999). Both, the observed and theoretical Balmer line profiles are normalised to the local continuum in a consistent manner. Wavelength shifts are calculated for the actual RV estimate for each spectrum. The synthetic spectra are convolved to the observational resolution with a Gaussian and interpolated to the actual parameters with bi-cubic splines and interpolated to the observed wavelength scale.

Parameters are determined by minimising χ^2 . The optimisation is done by means of a simplex algorithm, which is based on the AMOEBA routine of Press et al. (1992). The advantages of this approach are a high degree of stability and flexibility. New functions and parameters can be easily integrated. One disadvantage is that the convergence of simplex algorithms is not very fast and thus CPU time intensive. However, in practice this is not a major limitation for line profile fitting with FITSB2.

FITSB2 offers a number of options for fitting line profiles: model spectra, Gaussians, Lorentzians, and polynomials or a combination of these four. Most white dwarf spectra were simply fitted using model profiles calculated for the appropriate parameters. The default fit interval was $\pm 15 \text{ \AA}$ relative to the line centre. However, sometimes it was appropriate to use larger wavelength intervals. The intervals were adjusted according to the measured RVs. In a number of cases the model line profiles did not give a satisfactory fit of the observed spectra, potentially compromising the accuracy of the measured RV. If that happened Gaussians,

Lorentzians and/or polynomials were used to improve the fit; see Sect. 4 for a discussion and examples.

Our observational set-up results in vastly oversampled spectra. Moreover, Doppler broadening results in a substantial broadening of the NLTE line cores of the H α and H β (the Doppler width of H α at 10 000 K is 2.2 \AA). This allowed us to use a simple method to estimate the local noise. A moving parabola was fitted to 20 pixels and the standard deviation computed. This was repeated for all pixels. Afterwards, the pixel by pixel standard deviations were smoothed by a 50 pixel boxcar.

Radial velocity errors were calculated using bootstrapping. This method randomly selects N points of the N points of the observed spectra. Points can be selected more than once, which has the effect that on average $1 - e^{-1}$ points of the original spectrum are represented in the new spectrum. Radial velocities are refitted using the bootstrapped spectrum. This process is repeated and the errors are computed from the standard deviation of the derived parameters. Error estimates using bootstrapping are better at taking into account uncertainties resulting from imperfections of the input data (e.g. hot or dead pixels) and non-Gaussian noise than standard estimates from the co-variance matrix.

Error estimates from bootstrapping are subject to statistical fluctuations and a sufficient number of bootstraps need to be done. The bias-corrected three step method of Andrews & Buchinsky (2000) is applied to estimate the number of necessary iterations. We required that the probability of the error estimates being wrong by more than 10% is less than 1%. The number of bootstraps depends on the distribution of bootstrapped parameters with long tails requiring more bootstrap steps to achieve the required accuracy. Our accuracy requirements resulted in a minimum of 332 bootstraps. Note that the parameters describing Gaussians, Lorentzians and polynomials modifying the model spectrum are treated as free parameters and thus enter the error budget.

4. Results

Survey spectra were taken for a total of 689 targets classified as DA. It turned out that the spectra of 46 stars revealed the presence of red companions (Koester et al. 2009), almost all M type main sequence stars, but also at least one brown dwarf (Maxted et al. 2006). The DA+dM nature of most of these targets was not known at the time they were scheduled for observations. For many of the white dwarfs only low quality classification spectra of the blue range existed, which did not allow the detection of the cool companion.

A further 18 targets could not be checked for RV variations, because only one spectrum was taken, leaving 625 white dwarfs we could analyse for RV variations and the presence of a compact companion. Our RV measurements of the 643 DAs without a cool companion are summarised in Table B.1. We applied heliocentric corrections to the velocities, but no corrections for gravitational redshift. The latter can exceed 100 km s^{-1} for high mass white dwarfs and need to be taken into account when calculating space velocities, but in this study the emphasis is on velocity variations.

We used the same criterion for variability as used by Maxted et al. (2000b). For each star a weighted mean of the RVs is computed. We then calculate χ^2 from the deviations of the individual RVs from the mean. χ^2 measures the goodness of fit of the ‘‘model assumption’’ of a constant RV. The comparison with a χ^2 distribution with the appropriate number of degrees of freedom yields the probability p of obtaining the observed value of χ^2 or higher from random fluctuations. The computed values of

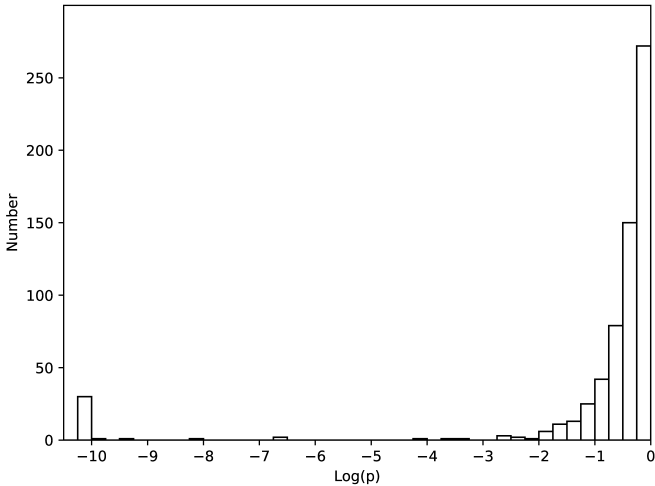


Fig. 5. Distribution of $\log p$ from Table B.1. The peak on the right represents statistical noise only. Our detection threshold is $\log p < -4$. Two systems have $-4 < \log p < -3$; the bin at $\log p = -10$ summarises all objects with $\log p \leq -10$; many of them have $\log p$ much less than this value.

χ^2 and $\log p$ are tabulated in Table B.1 and the distribution of $\log p$ is displayed in Fig. 5. We chose a detection threshold of $p < 10^{-4}$, that is white dwarfs with p values below this value are considered to be binaries (indicated as “DD”) in Table B.1. This limit corresponds to 0.1 expected false detections due to random chance in the complete SPY sample of ≈ 1000 white dwarfs and pre-white dwarfs. Two targets, WD 0032–317 and WD 1241–010, have $p < 10^{-3}$, indicative of a higher-than-average chance of their being binaries, but do not meet our $p < 10^{-4}$ criterion. WD 1241–010 is in fact a known DD (Marsh et al. 1995); WD 0032–317 could reward future study. Three targets did not show RV variations exceeding our detection threshold, but visual inspection identified them as double-lined systems, consisting of two white dwarfs. They are indicated by “dd” in Table B.1. See Sect. 4.4 for a discussion of individual objects identified this way.

When a combination of model atmosphere spectra with Gaussians, Lorentzians, and/or polynomials is used for the line profile fitting this is marked in the comments column of Table B.1. See Appendix B for a detailed description of the table.

4.1. Peculiarities

As stated above, the fits of the $H\alpha$ and $H\beta$ line make use of model atmosphere profiles. These are computed for the fundamental parameters derived from the fit of the entire Balmer line series as outlined in Koester et al. (2009). Thus in an ideal world the only free parameters during the fitting procedure would be the RVs. This worked well for about half of the programme stars (e.g. for HS 0002+1635 in the top left panel of Fig. 4). However, the fit between observed and synthetic line profiles was less than perfect for very hot and for cool white dwarfs.

4.1.1. Very hot white dwarfs

The hottest stars in the SPY sample displayed stronger emission cores than predicted by the models (example WD 2146–433; Fig. 4, top right). The problems are probably explained by the presence of metals in the atmosphere, which modify the atmospheric structure and thus the line profiles (Werner 1996). However, Latour et al. (2015) report that discrepancies still per-

sist, even if the correct abundances are adopted for model calculations and a good fit can only be achieved with arbitrarily increased abundances. We took the pragmatic approach of amending the cores of our model spectra by adding Gaussians and/or Lorentzians to achieve a good fit.

4.1.2. Cool white dwarfs

Many cool DAs showed broader and stronger line cores than predicted by the models (e.g. WD 0126+101; Fig. 4, bottom left). Koester et al. (1998) reported on the presence of flat bottom profiles of the cores of $H\alpha$ for pulsating white dwarfs of the ZZ Ceti type. The reason for these flat cores is very likely the velocity field associated with the pulsations (Koester & Kompas 2007). Similar and even stronger effects are present in our sample for a number of cool white dwarfs outside the ZZ Ceti instability strip (WD 0126+101 has a temperature of 8557 K; Koester et al. 2009). One can speculate that the reason of this discrepancy are violent convective motions in the atmospheres as seen in hydrodynamic models (Tremblay et al. 2013).

A more detailed comparison with models could give interesting insights, but here we took again a pragmatic approach and combined the model atmosphere spectra with Gaussians, Lorentzians, and/or polynomials to achieve a good fit of the line cores.

4.1.3. Magnetic white dwarfs

The SPY sample includes ten magnetic white dwarfs, most of them new discoveries based on the Zeeman splitting of the Balmer lines (Koester et al. 2009). Our model spectra do not include the effects of magnetic fields. We simply modelled the observed spectra as well as possible using combinations of Gaussians and Lorentzians (see WD 1300–098; Fig. 4, bottom right). This is a rather crude and unphysical approach, but once a good reproduction of the line profiles is achieved, accurate RV velocities can be measured. Note that the absolute velocities measured this way, should be treated with caution. For that the measurements should be repeated with a proper treatment of the magnetic fields. None of the magnetic white dwarfs displayed any RV variation.

4.1.4. Spectral types DAB and DAO

Four of the white dwarfs in our sample are of spectral type DAB and two of spectral type DAO (HE 1106–0942³ and WD 1305–017) showing lines of He I or He II, respectively in addition to the hydrogen lines. We used NLTE atmospheres computed for a mix of hydrogen and helium for analysing the DAOs.

HS 0209+0832 is a genuine DAB white dwarf showing helium line profile variations (Heber et al. 1997b). Two other DABs (WD 0128–387 and WD 0453–295) were analysed by Wesemael et al. (1994), who showed that a consistent fit of lines and spectral energy distribution is only achievable with a composite spectrum combining a hydrogen-rich and a helium-rich WD. Similarly, Bergeron & Liebert (2002) found WD 1115+116 to be a DA+DB double-lined binary system from a model atmosphere analysis. This was confirmed by Maxted et al. (2002)’s measurement of a 30 day orbital period, the longest measured for any DD. A detailed decomposition of the spectrum is beyond

³ This star is amongst the hottest and is the most luminous star in our sample. Stroeger et al. (2007) classified it as a subluminescent O star (sdO) and derived atmospheric parameters similar to those listed in Table C.2.

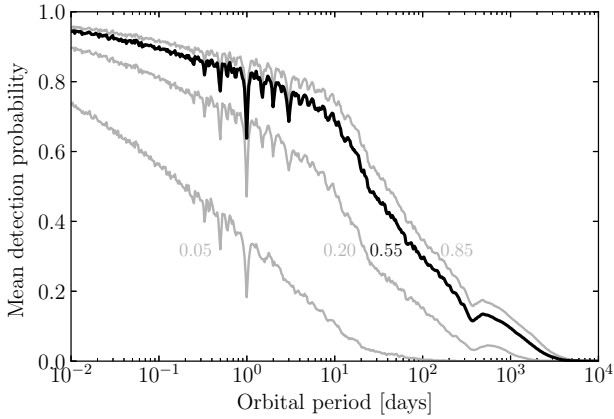


Fig. 6. Mean detection probability of the 632 targets with more than one RV in our sample as a function of orbital period, including 7 additional targets from Maxted et al. (2000b) that satisfy the SPY survey criteria. Dips in efficiency at e.g. $P = 1$ d correspond to typical time intervals between exposures. The calculations were based on the assumption that the visible white dwarf has a mass of $0.55 M_{\odot}$ and companion masses of 0.05 (brown dwarf), 0.20 (ELM), 0.55 (typical white dwarf) and $0.85 M_{\odot}$ (Chandrasekhar mass system) as indicated on the plot.

the aims of this investigation and the He I lines are weak. We fitted the hydrogen-rich component with a DA model atmosphere and used Gaussians to fit He I lines. We included only the 4713.3 \AA , 5015.7 \AA and 5875.8 \AA lines not displaying strong forbidden components. Results for the DABs will be discussed in Sect. 4.4.

4.2. Detection efficiency

The mean detection efficiency of the SPY sample is plotted in Fig. 6. For each star observed, the detection probability was evaluated as a function of orbital period using the same times and radial velocity uncertainties as observed along with the 0.67 km s^{-1} uncertainty added in quadrature that we discussed earlier. The probabilities were obtained by calculating the critical orbital inclination i_c for which our $\log p = -4$ threshold was met, and then using $P(i \geq i_c) = \cos(i_c)$ on the assumption of randomly inclined orbits. Random orbital phase offsets were accounted for by averaging over a uniform grid of 20 initial orbital phases in each case. We included the radial velocities measured by Maxted et al. (2000b) for ten targets that fulfil the SPY criteria but which we had excluded from the survey because of the earlier study. Three of these targets were in fact re-observed in SPY and so the combined datasets were used for these. The remaining seven were a small addition to overall sample, to give a total of 632 targets.

The detection probability of a given DD depends upon the masses of the component stars. We assumed a mass of $M_1 = 0.55 M_{\odot}$ for the dominant primary star, while the assumed companion mass M_2 differentiates the different lines plotted in Fig. 6; the lines shown are invariant for constant values of $M_2^3 / (M_1 + M_2)^2$. The key point of the plot is that SPY has good sensitivity over all of the known range of DD orbital periods. For typical orbital periods of DDs of around a day and normal mass white dwarf companions, the detection probability is of order 80%, while it exceeds 90% for periods of a few hours or less. The high precision of the SPY velocities means that there is even significant sensitivity to orbital periods as long as 100 days or more. Low mass companions cause lower amplitude RV

changes, and so the detection probability drops significantly for brown dwarf mass companions ($M_2 \sim 0.05 M_{\odot}$), but, since all known examples of unresolved white dwarf/brown dwarf binaries are of short period (Parsons et al. 2017), ~ 10 h or less, SPY has significant sensitivity to such systems as well. Calculations such as those of Fig. 6 could be used to correct for DDs missed in SPY (WD 1241–010 is one such system; Marsh et al. 1995), but we refrain from doing this as the correct approach is a more nuanced multi-dimensional problem that allows for multiple selection effects when comparing theoretical and observational populations, which we discuss in more detail in Sect. 5.2.

4.3. DA white dwarfs with Ca II lines

A number of DA white dwarfs observed by SPY display Ca II absorption lines (Koester et al. 2005a) and are thus of spectral type DAZ. The most prominent features are the Ca II H and K resonance lines. These lines are much narrower than the H α and H β Balmer lines used by us and the Ca K line is well suited for accurate RV measurements. The other component of the doublet, Ca H, is usually too strongly disturbed by the nearby strong He line to be useful.

The Ca II lines are broadened by quadratic Stark (and eventually neutral) broadening, which both lead to small asymmetries and line shifts. This could be a potential problem in particular, when lines are very strong, but if χ^2 is small then we can be confident that the impact is too small to make a noticeable effect.

Nine of the DA white dwarfs of the sample presented show detectable Ca II lines of photospheric origin. This was established by Koester et al. (2005a) from a comparison of the RV measured from the calcium lines and the Balmer lines. Interstellar Ca lines are present in the spectra of some hotter white dwarfs.

Here we will use the photospheric Ca lines to check the internal consistency of the RV measurements. While the H α and H β lines are registered with the two CCDs in the red channel of UVES, the Ca K lines are observed with the third CCD in the blue channel. CCD specific problems or systematic errors during the spectral reduction process and RV measurement should show up in a comparison.

Results for the Ca K line and the corresponding Balmer line measurements are listed in Table 1 and a plot of the resulting differences is shown in Fig. 7. The agreement is very good. Only two values out of the 19 in Fig. 7 show deviations exceeding the 1σ limits computed from the individual error limits. The resulting reduced χ^2 amounts to 0.72, well in agreement with purely statistical scatter. We conclude that SPY was routinely able to measure radial velocities of white dwarfs at the few km s^{-1} level, and, on brighter targets, to well below 1 km s^{-1} .

4.4. Double degenerates

Our RV measurements are summarised in Table B.1. RV variable DDs are indicated by “DD”. We detected a total of 39 DDs (see Table 2 for more details). Of these, 19 are single-lined (SB1) and 20 double-lined (SB2). For ten of the SB2 systems radial velocity curves have been measured and masses of the components derived. Ten SB2 systems are still awaiting follow-up spectroscopy. Similarly, for nine SB1 systems radial velocity curves have been measured and minimum masses of the components derived. Four of these DDs have been published in previous works not related to SPY, while three others have orbits presented in papers unrelated to SPY but subsequent to their detection as DDs in SPY – see Table 2 for references.

Table 1. Radial velocities $v(\text{Ca})$ measured from photospheric Ca K lines compared to the Balmer line values $v(\text{H})$.

Object	Date	UT	$v(\text{Ca})$ (km s^{-1})	$v(\text{H})$ (km s^{-1})
WD 0408–041	15/09/00	09:28	19.2 ± 1.5	19.8 ± 1.3
	02/09/01	09:17	17.4 ± 2.0	18.7 ± 1.7
WD 1124–293	23/04/00	03:55	29.4 ± 1.5	29.5 ± 0.7
	17/05/00	02:07	29.3 ± 2.2	29.2 ± 1.5
WD 1150–153	23/04/00	04:27	23.7 ± 1.1	28.4 ± 1.5
	19/05/00	01:23	19.3 ± 0.9	22.6 ± 1.4
WD 1202–232	23/04/00	04:44	22.6 ± 2.3	23.1 ± 0.3
	17/05/00	03:08	25.1 ± 2.3	23.6 ± 0.4
WD 1204–136	23/04/00	04:54	37.5 ± 1.1	37.5 ± 1.4
	17/05/00	03:31	35.3 ± 1.7	38.1 ± 3.2
HE 1225–0038	22/04/00	02:44	11.6 ± 2.4	10.6 ± 0.7
	17/05/00	03:44	10.7 ± 3.0	12.1 ± 1.4
	04/07/00	23:28	13.2 ± 3.4	11.1 ± 0.6
HE 1315–1105	23/04/00	01:30	32.1 ± 2.5	31.9 ± 1.0
	19/05/00	03:08	31.4 ± 2.3	31.5 ± 1.3
WD 1457–086	13/07/00	04:07	20.5 ± 3.6	22.9 ± 2.0
	16/07/00	02:03	21.4 ± 3.0	19.4 ± 1.6
WD 2326+049	06/08/00	04:18	43.4 ± 0.7	44.4 ± 1.1
	17/09/00	04:02	39.3 ± 0.5	39.8 ± 1.2

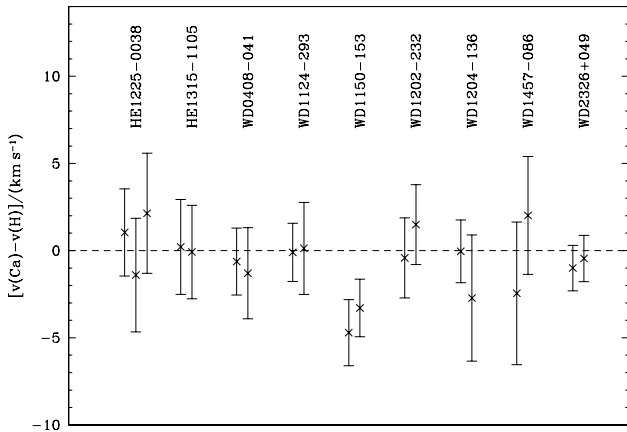


Fig. 7. Differences between $v(\text{Ca})$ and $v(\text{H})$ for the individual spectra as listed in Table 1. Error limits are computed by combining the error estimates for the lines in quadrature.

Figure 8 shows the distribution of our single white dwarfs in the $T_{\text{eff}}/\log g$ plane. Double degenerates are shown in Fig. 9. The fundamental parameters and their sources are listed in Appendix C.

4.5. Double-lined systems

In Fig. 10 we show spectra of 18 of the 20 double-lined DDs found in the survey, excluding only the two DAB white dwarfs, WD 0128–387 and WD 1115+166, which we discuss below. Double-lined systems are of particular interest since, once fully characterised, they deliver mass ratios and fundamental parameters for both stars and thus are of special importance for the understanding of the prior evolution of the systems. We now discuss special cases.

WD 2020–425: The spectrum shown in Fig. 10 appears to show only the $\text{H}\alpha$ core of one object. However, comparison of

the two spectra taken at different epochs (Fig. 11) demonstrates the existence of a second component. This white dwarf is in the parameter range described before (Sect. 4.1), in which $\text{H}\alpha$ has neither an absorption nor an emission core. WD 2020–425 has parameters, which make it a possible SN Ia progenitor (Napiwotzki et al. 2005). Its period is short enough to let it merge within a Hubble time and the combined mass of both white dwarfs is very close to the Chandrasekhar limit. However, the lack of a sharp core of the second, high mass, white dwarf results in relatively high uncertainties, so that a mass below Chandrasekhar can not be ruled out.

HS 0237+1034: No second epoch survey spectrum exists for HS 0237+1034. However, it is a double-lined DD consisting of two DA white dwarfs (Fig. 10).

MCT 0136–2010: Two spectra were taken for this target. The RV shift measured between the two spectra is not significant. The reason for us to classify it as DD is its double-lined spectrum. This is not too obvious at a first glance at Fig. 10. However, the two spectra taken at different epochs (Fig. 12) are clearly different and the χ^2 difference between a fit with and without a second component is 130.5, highly significant. Figure 12 shows the $\text{H}\alpha$ profile fitted with a single model.

The small RV offsets in both epochs makes a small RV amplitude and thus a long period likely. Although it is thus unlikely to qualify as SN Ia progenitor, it appears to have a high mass. The fundamental parameters derived by Koester et al. (2009) from a single-lined fit are $T_{\text{eff}} = 8416 \text{ K}$ and $\log g = 8.405$, making it an interesting object for further follow-up.

Spectral types DAB and DAO: Two of the DABs (WD 0453–295 and WD 1115+166) show large RV variations and are clearly short period DDs. The spectrum of WD 0453–295 shows two $\text{H}\alpha$ components making this a DA+DBA binary. No second $\text{H}\alpha$ component is visible in WD 1115+166 and it is thus a DA+DB binary, in agreement with the detection of the binary period and anti-phased motion in the hydrogen and helium lines by Maxted et al. (2002). The RV shift measured for WD 0128–387 has barely 1σ significance. However, we noted that in our spectra the He I lines of the DB component are blueshifted by $60\text{--}70 \text{ km s}^{-1}$ relative to the Balmer lines. The Balmer lines show a weaker blueshifted component, too. This could be explained by gravitational redshift, if the DA were the more massive white dwarf in the system. However, according to the model atmosphere analysis of Wesemael et al. (1994) the DB has higher gravity ($\log g = 9.0$) than the DA ($\log g = 8.5$) thus ruling out gravitational redshift as explanation. We conclude that, although the evidence is somewhat circumstantial, WD 0128–387 is a close DD system consisting of a DA and a DBA. No significant RV variations were detected for the two DAOs HE 1106–0942 and WD 1305–017 included in the SPY sample.

4.6. Notes on individual objects

WD 1845+019: This object is listed as a white dwarf with a cool companion candidate in Hoard et al. (2007). The authors find this white dwarf has a near-IR excess in Two Micron All Sky Survey (2MASS, Skrutskie et al. 2006). Maxted & Marsh (1999) found spectroscopic evidence for a long-period, red companion inferred from the presence of narrow, stationary emission near the core of $\text{H}\alpha$. The SPY spectra show similar emission at $\text{H}\alpha$, whereas Schmidt & Smith (1995) did not report any sign of such emission from spectra which also covered $\text{H}\alpha$. It is not known whether the close neighbour star described by Debes et al. (2005) is gravitationally bound to the white dwarf and whether it is the

Table 2. DDs identified in this survey.

Object	$\log p$	Type	M_1 (M_\odot)	M_2 (M_\odot)	P (d)	References
WD 0028–474	<–100	SB2	0.54	≥ 0.46	0.39	SPY: Koester et al. (2009), Napiwotzki et al. (2007). Rebassa-Mansergas et al. (2017)
WD 0037–006	<–100	SB2	0.51			
WD 0101+048	–17.54	SB1	0.49			
WD 0128–387	–0.48	SB2	0.85			
HE 0131+0149	–9.47	SB1	0.50			
WD 0135–052	<–100	SB2			1.56	Mass could not be derived (see Sect. C); Saffer et al. (1988), Bergeron et al. (1989)
MCT 0136–2010	–0.39	SB2	0.86			
HE 0205–2945	–4.07	SB2	0.41			
WD 0216+143	–6.75	SB1	0.54			
HE 0225–1912	–28.02	SB2	0.55	0.23	0.22	SPY: Napiwotzki et al. (2007)
HS 0237+1034	0.00	SB2	0.67			
HE 0315–0118	<–100	SB2	0.50	0.49	1.91	SPY: Koester et al. (2009), Napiwotzki et al. (2007). Rebassa-Mansergas et al. (2017)
HE 0320–1917	–42.87	SB1	0.31	≥ 0.45	0.86	SPY: Nelemans et al. (2005), Koester et al. (2009)
HE 0324–1942	–8.18	SB2	0.78			
HE 0325–4033	–9.86	SB1	0.49			
WD 0326–273	<–100	SB1	0.36	≥ 0.96	1.88	SPY: Nelemans et al. (2005), Koester et al. (2009)
WD 0341+021	<–100	SB1	0.38			Probably long period, Maxted et al. (2000b)
WD 0344+073	–19.26	SB1	0.39			
HE 0410–1137	–40.63	SB2	0.49	0.36	0.51	SPY: Napiwotzki et al. (2007). Rebassa-Mansergas et al. (2017)
WD 0453–295	<–100	SB2	0.40	0.44	0.36	SPY: Karl (2004), Napiwotzki et al. (2007)
HE 0455–5315	–66.18	SB1	0.47			
WD 1013–010	–39.55	SB1	0.32	≥ 0.62	0.44	SPY: Nelemans et al. (2005), Koester et al. (2009)
WD 1022+050	<–100	SB1	0.37	> 0.28	1.16	Maxted & Marsh (1999), Morales-Rueda et al. (2005), Nelemans et al. (2005)
HS 1102+0934	–47.41	SB1	0.38	≥ 0.45	0.55	SPY: Nelemans et al. (2005), Koester et al. (2009). Brown et al. (2013)
WD 1115+166	–22.28	SB2	0.69	≥ 0.52	30.1	Maxted et al. (2002)
WD 1124–018	<–100	SB1	0.49			
WD 1210+140	<–100	SB1	0.33	≥ 0.44	0.64	SPY: Nelemans et al. (2005), Koester et al. (2009)
HS 1334+0701	–6.51	SB1	0.35		0.23:	SPY: Karl (2004), period ambiguous
WD 1349+144	–53.30	SB2	0.53	0.33	2.21	SPY: Nelemans et al. (2005), Koester et al. (2009)
HE 1414–0848	<–100	SB2	0.52	0.74	0.52	SPY: Napiwotzki et al. (2002), Morales-Rueda et al. (2005), Nelemans et al. (2005)
HE 1511–0448	–17.85	SB1	0.50	≥ 0.67	3.22	SPY: Nelemans et al. (2005), Koester et al. (2009)
WD 1824+040	<–100	SB1	0.40	≥ 0.73	6.27	Saffer et al. (1998), Morales-Rueda et al. (2005), Nelemans et al. (2005)
WD 2020–425	<–100	SB2	0.81	0.54	0.30	SPY: Koester et al. (2009), Napiwotzki et al. (2007)
WD 2200–136	<–100	SB2	0.46			
HE 2209–1444	–38.47	SB2	0.43	0.72	0.28	SPY: Karl et al. (2003), Morales-Rueda et al. (2005), Nelemans et al. (2005)
HS 2216+1551	–99.25	SB2	0.64			
WD 2330–212	–27.79	SB1	0.45			
WD 2336–187	–16.23	SB2	0.36			
HE 2345–4810	–15.62	SB1	0.43			

Notes. References are provided for those that have previously been identified as DDs, in many cases from the SPY survey. The probability of a false positive, type and mass of the primary M_1 is given (see Appendix C). M_2 and P are secondary masses and periods determined by follow-up observations.

same as the companion star inferred by Maxted & Marsh (1999). This object was erroneously listed in Koester et al. (2009) as a double degenerate. We measured RVs modelling $H\alpha$ as a composite of a DA spectrum and a Gaussian emission. Our measurements have small error bars and are consistent with constant velocities.

WD 2359–434: The line cores of this white dwarf have a strange flat profile with a weak narrow component already reported in Koester et al. (1998). Koester et al. (1998) speculated that WD 2359–434 is magnetic and that what they see is only the unshifted component of the Zeeman triplet, with the other components shifted outside their observed spectral range or smeared out due to the inhomogeneity of the field. Aznar Cuadrado et al. (2004) included this object in their spectropolarometric observations and discovered a weak magnetic field of 3 kG. However, our spectra do not show any shifted Zeeman

components. A complicated field structure could smear out the shifted components, but a 3 kG field would be too weak to produce smearing over the necessary wavelength range.

Landstreet et al. (2012) reanalysed UVES and FORS data of this object and detected a non-uniform magnetic field in the range 3.1–4.1 kG. On the other hand, Kawka & Vennes (2012) obtained a magnetic field of 9.8 kG from spectropolarometric observations.

Infrared spectroscopy puts very tight constraints on any cool main sequence or substellar companion (Dobbie et al. 2005). Even brown dwarfs with a spectral type earlier than T8 (corresponding to a mass of $0.05 M_\odot$ for an age of 10 Gyr) can be ruled out. No sign of an infrared excess produced by warm circumstellar dust can be seen in the J , H and K bands.

For our RV measurements we modelled the flat bottom line profiles assuming fast rotation and broad Lorentzians, i.e. the

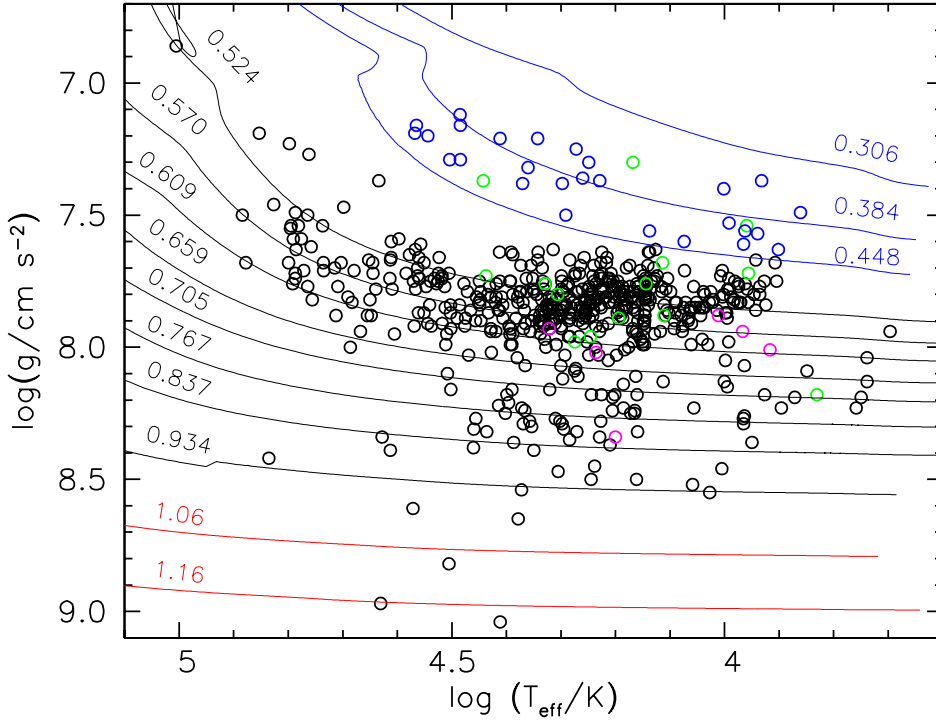


Fig. 8. Comparison of the SPY sample to evolutionary tracks in the $T_{\text{eff}} - \log g$ plane. Tracks for He-core WDs in blue (Pani et al. 2007), for C/O core WDs in black (Renedo et al. 2010) and for O/Ne core white dwarfs in red (Althaus et al. 2005). The tracks are labelled with their mass. Positions of all stars in Table C.2 excluding the DD white dwarfs and stars without a mass determination. Magnetic white dwarfs are shown in magenta, those with only one spectrum in Table B.1 in green. The hot, low gravity star HE 1106–0942, the high gravity DA WD 0346–011, and the magnetic, high gravity DA WD 2051–208 are off-scale.

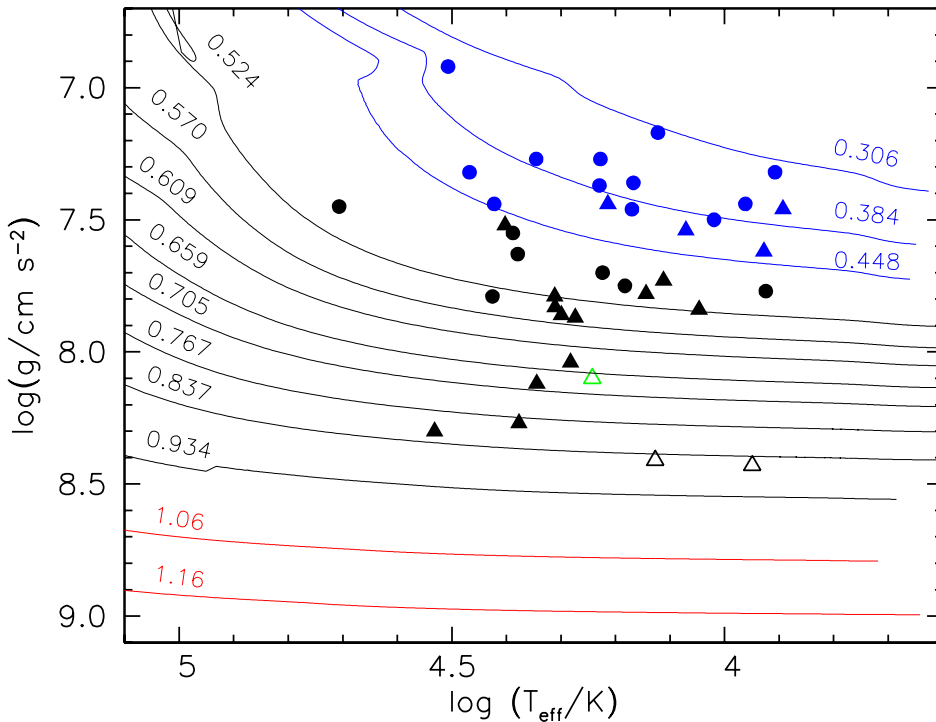


Fig. 9. Comparison of the DD SPY sample to evolutionary tracks. See Fig. 8 for details. SB1 systems (19) are shown as filled circles and SB2 systems (19) as triangles; the SB2 WD 0135–052 is not shown as we were not able to determine masses for it. Filled triangles mark systems that are RV variable, while open ones label SB2 systems that were found by visual inspection of their spectra, but are not considered RV variable (WD 0128–387 and MCT 0136–2010) or where only one spectrum was taken (HS 0237+1034). The parameters of the brighter component were used. The gravity of HE 0225–1912 has been offset by -0.05 dex to improve visibility.

narrow component was ignored. Our assumption of fast rotation is only an attempt to model the profile and does not imply that WD 2359–434 is really a fast rotator. Our spectra, taken four days apart, do not show a significant RV shift.

4.7. Magnetic white dwarfs

Ten magnetic white dwarfs have been identified in the SPY survey by Zeeman splitting. WD 0058–044 and WD 0239+109 were already published by Koester et al. (2001). HS 0051+1145, HE 1233–0519 and WD 2051–208 were first identified in SPY and details can be found in Koester et al. (2009). Three other

magnetic white dwarfs (WD 0257+080, WD 1953–011 and WD 2105–820) were studied by SPY, confirming their magnetic nature, but were already published in previous works. More information on these objects can be found in Koester et al. (2009). Further to these objects in this work we have also identified two other magnetic white dwarfs that were already published (WD 1300–098 and WD 1350–090). More details on these two objects are given below.

WD 1300–098: The SPY spectra of this object showed Zeeman splitting in the Balmer lines (Koester et al. 2009). This was later confirmed in Gianninas et al. (2011).

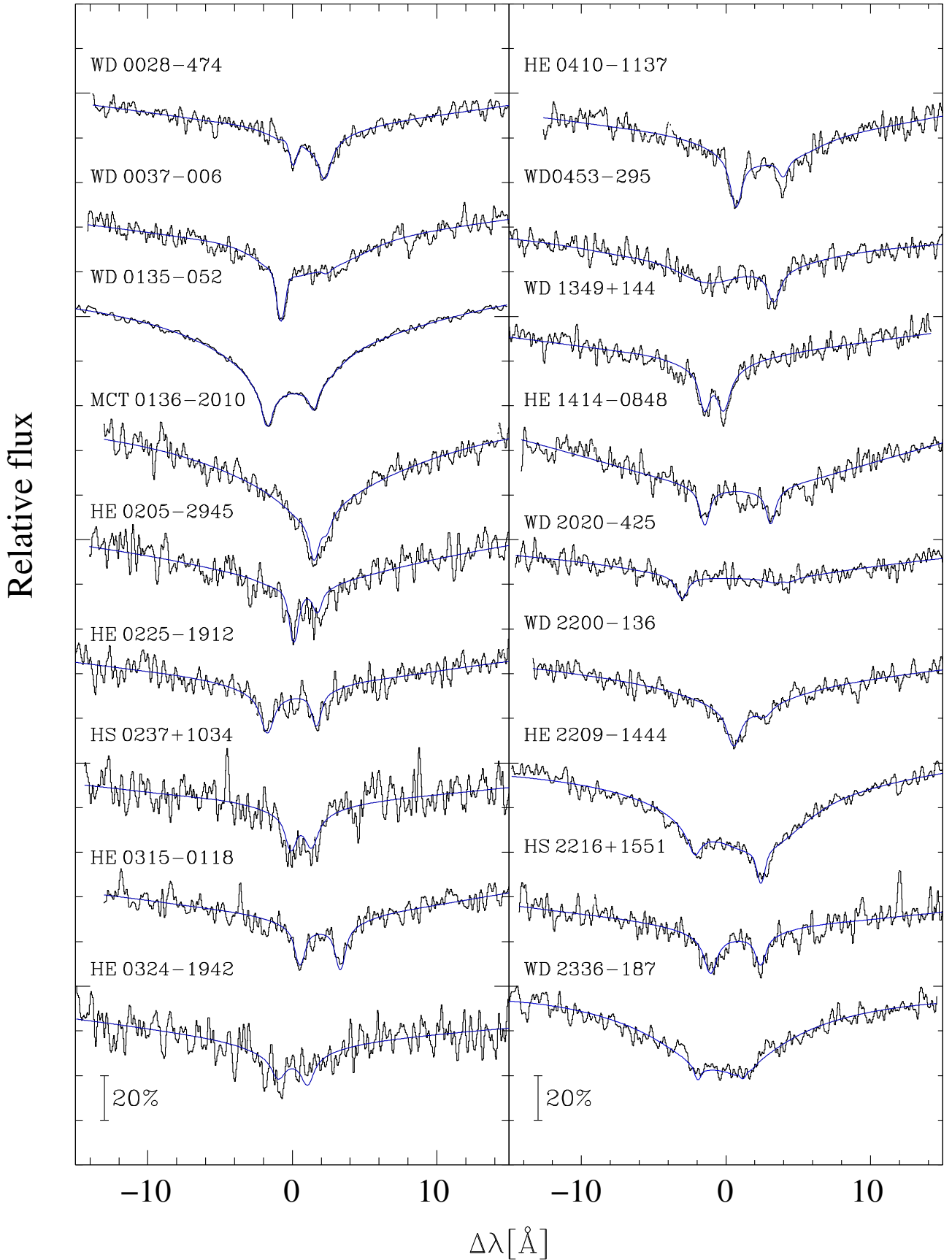


Fig. 10. $H\alpha$ region of 18 of the 20 the double-lined systems detected in the survey. Each system shown displays two $H\alpha$ cores; the two systems excluded, WD 0128-387 and WD 1115+166, are DABs and show only a single component at $H\alpha$. The figure shows one observed spectrum for each binary along with the best fitting model spectrum (blue smooth line). The observed spectra were smoothed with a Gaussian with 0.15 \AA for display. $\Delta\lambda$ is the wavelength offset relative to the laboratory wavelength of $H\alpha$.

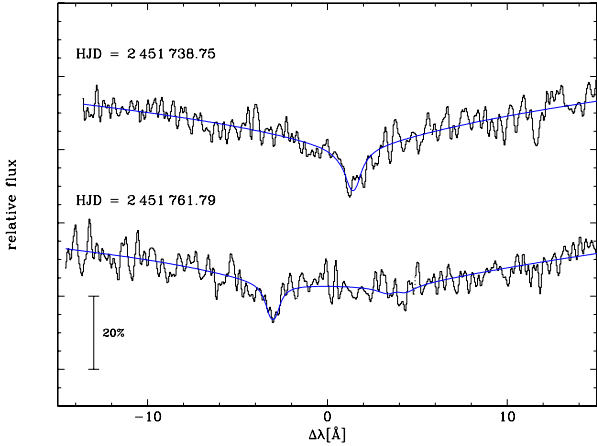


Fig. 11. $H\alpha$ region of the two spectra of WD 2020–425 taken at different epochs.

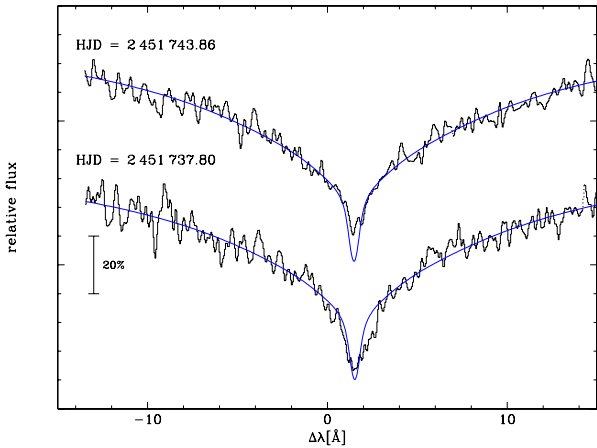


Fig. 12. $H\alpha$ region of the two spectra of MCT 0136–2010 taken at different epochs fitted assuming a single-lined spectrum.

WD 1350–090: This is a well known magnetic white dwarf which was found through spectropolarimetry to have a weak magnetic field of 85kG (Schmidt & Smith 1994). Wellhouse et al. (2005) studied the NIR values of this object looking for companions, but did not find one. The Zeeman splitting in the Balmer lines of the SPY spectrum of this white dwarf was first reported in Koester et al. (2001).

4.8. Comparison with Maoz & Hallakoun (2017)

Maoz & Hallakoun (2017) presented a similar analysis of a subsample of 439 DAs out of the 615 SPY DAs analysed by Koester et al. (2009). We start from 643 stars of which 18 have one spectrum only, leaving us with 625 stars. Hence, the sample of Maoz & Hallakoun (2017) is a subset of ours.

The criteria employed to identify radial velocity variables differ significantly between our two studies. While we use the $\log p < -4$ detection threshold (see Sect. 4), Maoz & Hallakoun (2017) prefer $\Delta RV_{\max} > 15 \text{ km s}^{-1}$ to identify a radial velocity variable star and $10 < \Delta RV_{\max} < 15 \text{ km s}^{-1}$ for candidates. We confirm all of the Maoz & Hallakoun (2017)’s detections except for HE 0516–1804 ($\log p = -0.72$), HS 2046+0044 ($\log p = -2.54$), and WD 0032–317, although as discussed earlier, this latter object could well prove to be a DD given its false alarm probability of $\log p = -3.74$.

We find ten stars to be radial velocity variable which are not listed in Maoz & Hallakoun (2017): the known SB2 systems HE 0315–0118, WD 0453–295 and WD 1115+0934, the known SB1 systems WD 0216+143, WD 0101+048, WD 1022+050, and HE 1511–0448 as well as the SB1s HE 0455–5315, HS 1334+0701, and HE 2345–4810. These objects are probably among their rejects. In addition, visual inspection of the UVES spectra allowed us to identify MCT 0136–2010 and HS 0237+1034 as SB2 systems (see Fig. 10).

Amongst Maoz & Hallakoun (2017)’s candidate RV variable objects ($10 < \Delta RV_{\max} < 15 \text{ km s}^{-1}$), we confirm that HS 2216+1551 is a radial velocity variable SB2 system, however, all 15 remaining candidates listed in their Table 1 are rejected using our criterion.

In summary, we reject 17 out of the 43 DDs of Maoz & Hallakoun (2017), confirming only 25 of them. Of these, 7 have system parameters published by the SPY consortium before, and 3 from other sources. From our full sample we identified 39 DDs including 20 SB2 systems. We identify 12 SB1 and 13 SB2 systems in the Maoz & Hallakoun (2017) subsample. However, the overall DD fraction in both samples is the same at 6%, if the same variability test is applied.

The ΔRV_{\max} statistic employed by Maoz & Hallakoun (2017) has two intrinsic weaknesses which could perhaps have contributed to the differences between our studies. First it takes no account of the number of spectra – the expected distribution of ΔRV_{\max} from purely statistical fluctuations always shifts towards larger values as the number of spectra considered increases. For instance, we find that a threshold that is only exceeded by chance 1% of the time with two spectra, is breached almost three times as often with three spectra, a purely statistical and spurious effect. There are perhaps indications in Maoz & Hallakoun (2017)’s results of the influence this effect: three of their 16 candidates have three or more spectra in SPY, whereas only one such case would have been expected by random chance. The second problem with ΔRV_{\max} is that it takes no account of varying statistical uncertainties between spectra. These issues are why we employed Maxted et al. (2000b)’s χ^2 -based criterion.

5. Discussion

We have presented RV measurements of a set of 643 DA white dwarfs observed for the SPY programme and remaining after 46 binaries with cool companions were removed from the original sample of 689. We obtained two or more spectra for 625 of these targets, 632 including targets covered by Maxted et al. (2000b). This sample contains 39 DDs (20 of the SB2 type, 19 of the SB1 type), 35 of them new discoveries. The directly detected rate of DDs in SPY is thus $6.2 \pm 1.0\%$ (uncertainty is 1σ from the binomial distribution). There are likely to be an additional 5 or 6 DDs in our sample that we did not detect, given typical periods of a day and our mean detection probability (Fig. 6), but a deduction of the space density of DDs requires accounting for much more than just period selection, as we discuss below in Sect. 5.2, so we prefer for simplicity to quote just the numbers as observed.

5.1. Dependence of DD numbers on mass

The SPY sample is large enough to see some significant variations with mass. The limiting mass for a He white dwarf is set by the minimum mass for a helium core flash which increases from 0.43 to $0.49 M_{\odot}$ (Dorman et al. 1993; Sweigart 1994) with decreasing metallicity, although it is common to adopt a

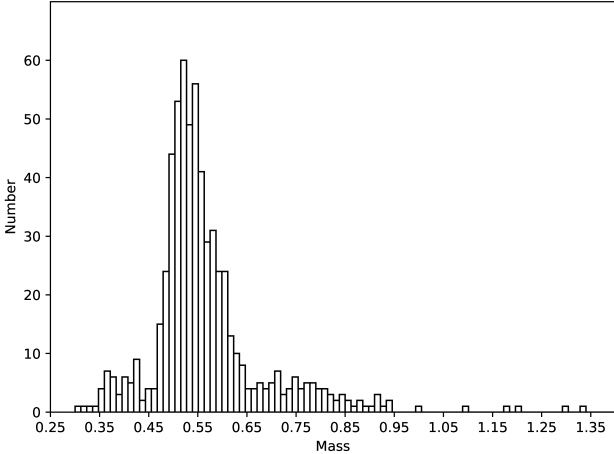


Fig. 13. Mass distribution of the SPY sample.

value of $0.45 M_{\odot}$. White dwarfs with higher masses usually have cores composed of carbon and oxygen. There are scenarios that lead to the formation of low-mass “hybrid” white dwarfs with C/O cores and thick helium mantles ($\sim 0.1 M_{\odot}$; [Iben & Tutukov 1985](#)). Some white dwarfs with masses around $0.45 M_{\odot}$ may also have evolved via the extreme horizontal branch (EHB), but these objects are also considered to be the product of close binary evolution (e.g. [Heber 2009, 2016](#); [Kupfer et al. 2015](#)). So low-mass white dwarfs may not always be helium core white dwarfs, although in all cases evolution within a binary is needed to model the early mass loss that prevents evolution towards a normal C/O WD.

Figure 13 displays the mass distribution of 615 DA white dwarfs of the SPY sample for which we could derive masses. The distribution may be four populations as suggested by [Kepler et al. \(2007, cf. their Fig. 8\)](#). To examine how DD numbers vary with mass, we consider those targets that (a) have masses in Table C.2 and (b) have two or more spectra and are thus sensitive to DDs. We arrive at the numbers listed in Table 3. All the DDs bar WD 0135–052, for which we could not determine a mass from SPY data, contribute to this table, i.e. 38 of the 39 DDs in SPY. We identify the 44 targets with primary masses $M_1 \leq 0.45 M_{\odot}$ (category I) as He white dwarfs. The dominant population II ($0.45 < M_1 \leq 0.65 M_{\odot}$) is identified with C/O-core white dwarfs. A third population of higher masses ($0.65 < M_1 \leq 1.0 M_{\odot}$) should also consist of C/O-core white dwarfs. A few white dwarfs have masses in excess of $1.0 M_{\odot}$ (population IV) and could include O/Ne-core white dwarfs and mergers in addition to C/O-core stars.

Of the 44 white dwarfs that have a mass below $0.45 M_{\odot}$, 16 show radial velocity variations indicating that they are double degenerates. In terms of detection probability, a set of $0.4 + 0.4 M_{\odot}$ DDs is comparable to (albeit a little below) the line corresponding to a companion mass of $0.55 M_{\odot}$ in Fig. 6. Thus, assuming periods of order a day, if all 44 were DDs, we would have expected to detect ~ 37 of them as such, ~ 33 if all companions were ELMs or low-mass main-sequence stars, and still ~ 20 to 26 for $0.05 M_{\odot}$ brown-dwarf companions with periods comparable to those discovered to date ([Parsons et al. 2017](#)). The observed number of 16 suggests that some of remaining 28 non-detections could be single, or be harbouring very low mass companions. It has been suggested that single low mass white dwarfs result from envelope loss induced by capture and spiral-in of planetary companions ([Nelemans & Tauris 1998](#)), or are the cores of red giants stripped by explosions of their companions

Table 3. Breakdown of targets with two or more spectra into four mutually exclusive sets defined by mass.

Type	I [0, 0.45]	II (0.45, 0.65]	III (0.65, 1.00]	IV (1.00, 1.40]
All	44	478	83	6
SB1	12	7	0	0
SB2	4	9	6	0

Notes. Exception: HS 0237+1034 has only one spectrum, but is double-lined. Notation: “[” or “]” – interval includes the limiting value; “(” or “)” – interval excludes the limiting value.

as supernovae ([Justham et al. 2009](#)), or are the products of mergers of components of cataclysmic binaries induced by frictional angular momentum loss following nova eruptions ([Zorotovic & Schreiber 2017](#)). All possibilities are interesting and these systems are worth further investigation.

The detection of 16 DDs amongst the 44 He white dwarf primaries is a fraction of $36.4 \pm 7.3\%$. By comparison, the 22 DDs in the remaining 567 systems with $M_1 > 0.45 M_{\odot}$, a fraction of just $3.9 \pm 0.8\%$, is a steep drop. For the dominant population of C/O white dwarfs (set II) the binary fraction is even lower (3.3%), while among the C/O white dwarfs of set III 7.2% are binaries. No binary was found among the white dwarfs with masses exceeding $1 M_{\odot}$ (set4). The He white dwarf DDs of set I divide 12:4 in favour of single-lined systems, while those of higher mass are skewed 7:15 towards double-lined systems (sets II–IV), in particular for set III, in which all six binary systems are double-lined. The dominant population of C/O white dwarfs (set II) divide almost equally. This is perhaps because low mass white dwarfs are large and will tend to dominate over their companions, but it could also be a consequence of the formation paths that result in these systems. There is useful potential here to constrain evolutionary models.

5.2. Selection effects in the SPY sample

The current sample of DDs has emerged from searches that often started with mass-dependent selection, following successful searches of the 1990s which concentrated upon low mass white dwarfs (e.g. [Marsh et al. 1995](#)). The most extreme example of this strategy is the ELM survey ([Brown et al. 2016a](#)) which uncovered targets so low in mass that they were not even recognised as white dwarfs when the SPY survey was undertaken. Such surveys are biased precisely against the high mass systems of most interest as type Ia progenitors, except to the extent that some may harbour high mass white dwarfs hidden in the glare of dominant low mass primary stars. They also focus on the extreme low mass wing of the white dwarf mass distribution, which is untypical of most systems. SPY is by far the most sensitive survey without mass selection built in from the start. Precursors to SPY were [Bragaglia et al. \(1990\)](#) and [Maxted et al. \(2000b\)](#) who surveyed 54 and 71 white dwarfs on 2–4 m-class telescopes, uncovering a handful of candidates, although the second of these studies emerged from searches that concentrated in the main upon low mass targets. The Sloan Digital Sky Survey (SDSS), although not designed for radial velocity work, serendipitously provides a very different type of constraint, providing a much larger sample, but also much looser radial velocity constraints. The SDSS is perhaps somewhat superior to SPY for finding massive, short-period type Ia progenitors ([Breedt et al. 2017](#)), but SPY is far more sensitive to the

bulk population of longer period and lower mass DDs. Moreover, SPY is particularly efficient in finding double-lined systems because of its high spectral resolution. At lower resolution such as the SDSS spectra, it is far more difficult because the components' line profiles are not resolved and the orbital motion will broaden the combined line profile rather than shifting the unresolved line centre. This is probably why double-lined DDs have not been found directly by the SDSS project. In addition visual inspection of SPY spectra allowed SB2 systems to be discovered that were considered RV non-variable by the detection criterion and, therefore, probably have long orbital periods. Hence, SPY will enable a more complete and reliable calibration of theoretical models. The two surveys are in many ways complementary to each other (Maoz et al. 2018), as can be judged from the detection probability plot for SDSS (Fig. 4; Breedt et al. 2017), comparable to Fig. 6 in this paper. The SDSS detection rate falls below 50% for $P > 0.2$ days, whereas SPY extends over 100 times longer, only dropping below 50% for $P > 30$ days. The numbers of DD detections in each survey corroborate this: the 6396 SDSS targets studied by Breedt et al. (2017) yielded 15 DDs, while we have found 39 DDs in 625 SPY targets. One can deduce ~ 400 other DDs in the SDSS sample that have yet to be detected as such.

The SPY sample was selected without regard to mass, but it inherits the selection effects of the input catalogues it was derived from, and accounting for these will be crucial when making comparisons to theoretical population models. A non-exhaustive list of such effects is: (a) period-dependent selection (Fig. 6), (b) selection by galactic location (Fig. 1), (c) colour selection, (d) selection by kinematics via proper motion surveys, and (e) selection by magnitude limits. All of these can be translated to a greater or lesser extent into mass-dependent selection functions. For instance, selection by temperature favours high mass targets since it takes longer for high mass white dwarfs to cool to 10 000 K than it does low mass white dwarfs, owing to a combination of available thermal energy and surface area. On the contrary, magnitude-limited surveys strongly favour low mass white dwarfs because of their greater size. There are also subtler effects such as mass-dependent kinematics (Wegg & Phinney 2012) which can lead to both proper motions and scale-heights varying with white dwarf mass. The correct way to allow for these effects is to impose them as closely as possible upon theoretically-derived samples rather than attempt to remove them from the observations. To this end we include a compilation of temperatures and gravities of the SPY sample along with *Gaia* IDs in Appendix C to facilitate future calculations. SPY-like samples can be generated from theoretical populations by selecting targets of similar colours and magnitudes and imposing in addition a similar selection by Galactic latitude. A full calculation would also simulate the detection of DDs along the lines of Rebassa-Mansergas et al. (2019). Such model-dependent calculations are far beyond our scope here where we aim instead to try to convey a feel for the level of the selection effects affecting the SPY sample, beyond the obvious ones of Galactic latitude and period discussed earlier.

Given the heterogeneous origins of the SPY input catalogue from a multitude of proper-motion, colour and objective prism surveys as well as serendipitous discoveries, it is close to impossible to unravel the selection effects of the original survey papers. Instead, we take advantage of the *Gaia* DR2 survey (Gaia Collaboration 2018) to quantify the extent of mass-dependent bias within the SPY sample selection as shown in Fig. 14.

We do so by choosing an approximately volume-limited subsample from *Gaia* as an approximation of what is naturally pro-

duced by population synthesis calculations. The parallax π and parallax error σ_π were restricted by $\pi > 10$ mas and $\pi > 5\sigma_\pi$ to give a near volume-limited sample to $d = 100$ pc, although there is still incompleteness in the lower part of the plot since $M_G > 14$ at 100 pc corresponds to $G > 19$. Unsurprisingly, the SPY sample⁴ is very differently distributed to the *Gaia* sample as shown in the Hertzsprung-Russell diagram on the left of Fig. 14. Above all, it is strongly skewed towards blue colours and high temperatures, reflecting the origins of the sample. The temperature selection automatically implies mass-dependent selection because of differential white dwarf cooling rates, as discussed above.

To judge the significance of additional mass-dependent selection biases, particularly that associated with the magnitude-limited input catalogues, we next look at the distribution of magnitudes across the main white dwarf cooling track, restricting ourselves to *Gaia* colours $G_{BP} - G_{RP} < 0$ to avoid a region of bifurcation in the *Gaia* H-R diagram believed to be associated with helium-dominated atmospheres (Gentile Fusillo et al. 2019). A polynomial fitted to these that was then subtracted from the *Gaia* and SPY targets to derive differential absolute magnitude histograms. (The differential effect of atmospheric composition in this region can be seen directly in Fig. 14 where our hydrogen-dominated DA sample clusters mainly along the upper of the two branches once $G_{BP} - G_{RP} > 0$.) The restriction in colour builds differential cooling mass-selection into the *Gaia*-selected reference sample too, so we are looking here for additional effects such as kinematic and magnitude bias. The key result is in the right-hand panel of Fig. 14 which shows that over-luminous targets ($\Delta M_G < -0.5$) are over-represented in SPY compared to a near-volume-limited *Gaia* sample, whereas faint systems ($\Delta M_G > +1$) are under-represented. This is as one would expect of a magnitude-limited sample, but the bias is slight compared to samples chosen for low mass, which are equivalent to applying the restriction $\Delta M_G < -0.5$ from the start. Translating Fig. 14 into a mass-bias is complex, since, while we can assume that $\Delta M_G > 0$ targets are more massive than average, double-lined systems with equal contributions from both components get a -0.75 magnitude boost, and could be reasonably massive but still end with $\Delta M_G < 0$. Such calculations are beyond our scope here as they would need to be made separately for any model population. The key point perhaps is that although the biases in the SPY sample are small compared to others in the literature, they are still significant and must be accounted for in any calculation of intrinsic DD fractions and merger rates.

Twenty of the 39 binaries found in SPY are double-lined, an astonishingly large fraction. As remarked above, double-lined systems are potentially up to 0.75 mag brighter than single white dwarfs of the same mass, boosting the chance that they are included in a magnitude-limited sample. Since the SPY sample was compiled from a number of catalogues and surveys with different faint limits, the survey does not have a well defined cut-off magnitude, however we can estimate the significance of the effect from the systems in hand. Figure 15 shows the probability of a white dwarf to be included in SPY. It was derived by comparing the brightness distribution of observed white dwarfs with a population produced using the model described in Napiwotzki (2009). Numbers of observed white dwarfs found in each bin are compared to the model predictions. Only relative probabilities are important. The probability is modelled with a simple linear

⁴ Apart from the following seven SPY targets that have either no parallax or no colour in *Gaia*: PG0922+162A, PG0922+162B, WD 1015+076, HE 1117-0222, WD 1121+216, WD 1147+255 and WD 1214+032.

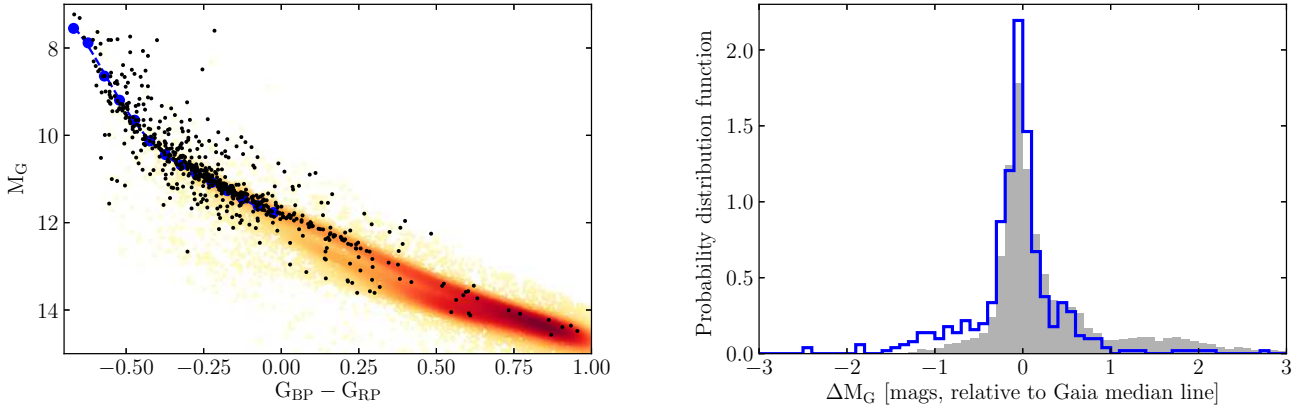


Fig. 14. *Left:* SPY sample (black dots) plotted in a Hertzsprung–Russell diagram (*Gaia* absolute magnitude versus *Gaia* colour) on top of a background of 11 561 white dwarf candidates selected from the *Gaia*-derived sample of [Gentile Fusillo et al. \(2019\)](#) and colour-coded by plot density. The large blue dots on the left mark the main cooling track of the *Gaia* white dwarfs for $G_{BP} - G_{RP} > 0$. The dashed line represents the polynomial fitted to the brightness distribution. *Right:* histograms of the differential magnitudes for *Gaia* (solid grey) and SPY (outline blue).

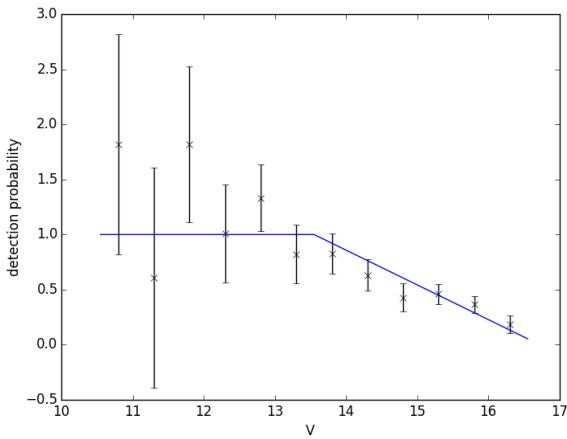


Fig. 15. Relative probability of a white dwarf being included in SPY as a function of brightness. Error bars are derived from the Poisson distribution.

function and assumed to be one for white dwarfs brighter than 13.55. The fitted probability p is

$$p = \begin{cases} 1.00 & V \leq 13.55 \\ 5.27 - 0.3154V & 13.55 \leq V \leq 16.55. \\ 0.00 & V > 16.55 \end{cases} \quad (1)$$

Fundamental parameters were determined by fitting the spectra with model spectra representing the two components (see Appendix C for details). We then calculated the contribution of the secondary star to the combined brightness and from that the brightness of the primary star alone. The probabilities of the system and the primary star alone were calculated using Eq. (1) and used to estimate the probability of the primary alone making it into the SPY sample. Example, if the probabilities are 60% and 30%, respectively, we count the system as 0.5. It turned out that 12.5 of the 20 double-lined binaries (63%) would have appeared in the survey. The total number of detected binaries would have dropped from 39 to 31.5 (81%).

5.3. Implications for SNe Ia progenitor scenarios.

Since the initiation of the SPY project, ideas about possible progenitors of SNe Ia have evolved considerably. In particular, the extensive work in following up SNe Ia has revealed

a richer diversity than was previously imagined ([Taubenberger 2017](#)). The most profound change perhaps has been a move away from the Chandrasekhar mass model, as there now seems to be good evidence for sub-Chandrasekhar ejecta masses in observed SNe Ia (e.g. [Scalzo et al. 2014](#)).

We note that among the objects already discovered by SPY there are two systems – WD 2020–425 ($M = 0.81 M_{\odot} + 0.54 M_{\odot}$, $P = 0.3$ d) and HE 2209–1444 ($M = 0.72 M_{\odot} + 0.43 M_{\odot}$, $P = 0.28$ d), which may well qualify as candidates for sub-Chandrasekhar SNe Ia progenitors. Moreover, the SPY project is not completed, as yet. Out of 39 DDs identified in the survey, only 19 have measured M_2 or lower limits thereof from RV curves. There are 10 SB2 DD still needing follow-up observations by UVES (see Table 2). The most interesting SB2 system to follow up is HE 0324–1942, because its primary mass ($\approx 0.8 M_{\odot}$) is as high as that of WD 2020–425.

The expectation of finding a super-Chandrasekhar pre-SN Ia white dwarf pair in the sample of about 1000 objects brighter than $V \approx 16^m.5$ was based on a count of the number of model systems satisfying the criteria $M_{\text{tot}} > M_{\text{Ch}}$ and $t_{\text{merger}} < t_{\text{Hubble}}$, while any selection effects were ignored. However, a numerical experiment modelling observations of a similar sample of white dwarfs by an instrument like VLT/UVES in which the effects of observational selection (orbital inclination, observational strategy, observing conditions, etc.) were taken into account ([Rebassa-Mansergas et al. 2019](#)), has shown that finding such a pair of white dwarfs may require a much larger sample of objects – they estimate a factor of ten. Given that the sample size of 643 presented in the paper does not match even the original aim of around 1000 targets (owing in the main to hot subdwarfs; [Lisker et al. 2005](#); [Stroeer et al. 2007](#)) which are hard to distinguish from white dwarfs from colours alone. Having also in mind a 20% loss due to detection efficiency, the SPY sample may well not deliver a super-Chandrasekhar, short period DD. However, with the switch of emphasis towards sub-Chandrasekhar mergers, it nonetheless retains its significance and is the only large survey sensitive to masses and periods typical of the bulk of the DD population.

The discovery of the DDs presented here is only a first step; the next is the determination of their orbital periods, which has been accomplished already in some cases, and should be a priority in future work on this sample. Once this is accomplished, we should be in a position to be able to compare the properties of DDs in samples generated through binary population synthesis

to an observed sample of relatively weak mass bias, and hence be able to judge on the SNe Ia rate that the Galactic population of DDs can plausibly sustain.

6. Summary

In this paper we have presented the methods and results of radial velocity measurements of 643 DA white dwarfs observed with UVES and the VLT as part of the SPY survey. We find 39 double degenerates in this sample, including 20 double-lined systems which show spectral components from both white dwarfs. One of the double-lined systems (WD 2020–425) is a candidate SN Ia progenitor with a total mass close to the Chandrasekhar limit, but the uncertainties of the mass for this binary are too large to be certain of this at present. The absolute radial velocities we presented will allow for future searches for long-period binarity, while the sample of DDs is well-suited for tests of binary population models.

The overall DD fraction in the SPY sample is 6%. We compared our results to the results of [Maoz & Hallakoun \(2017\)](#), who studied a subsample of the SPY data set and derived a DD fraction of $10\% \pm 2\%$ (1σ , random) $+2\%$ (systematic). We showed that their detection criterion for radial velocity variability is overly optimistic. Applying our detection criterion, we showed that 17 of their candidate DDs are unlikely to be RV variable, reducing their SPY subsample to 25 DDs. Accordingly, the DD fraction in the [Maoz & Hallakoun \(2017\)](#) subsample is in fact 6%, consistent as it should be with our result for the full SPY sample.

Our detected DD fraction among C/O white dwarfs is $3.9 \pm 0.8\%$, below the 10% fraction previously found, perhaps reflecting the prominence of low mass He white dwarfs in literature studies. The detected DD fraction amongst He white dwarfs in SPY is much higher at $36.4 \pm 7.3\%$, although it seems unlikely that all He white dwarfs are binary. We estimated that the number of binaries needs to be corrected by a factor of 0.8 to account for the increased probability of double-lined systems to be included in SPY, but there is a similar factor in reverse because our detection efficiency is 80 to 90% for typical DD periods, and a full comparison with theoretical models needs to take multiple selection effects into account, despite their being weaker in SPY than in any comparable survey. We provide the data needed to accomplish such a task.

Acknowledgements. We express our gratitude to the ESO staff, for providing invaluable help and conducting the service observations and pipeline reductions, which have made this work possible. TRM and SC were supported under grants from the UK's Science and Technology Facilities Council (STFC), ST/L00073 and ST/P000495/1. LRY is partially supported by Presidium of the Russian Academy of Sciences program P-28 and RFBR grant 19-02-00790. Work on the SPY project in Bamberg is supported by the DFG (grants Na365/2-1, Na365/2-2, HE1356/40-3 and HE1356/40-4). We thank Markus Dimpel for obtaining the *Gaia* IDs.

References

- Althaus, L. G., García-Berro, E., Isern, J., & Córscico, A. H. 2005, *A&A*, **441**, 689
- Andrews, D. W. K., & Buchinsky, M. 2000, *Econometrica*, **68**, 23
- Aznar Cuadrado, R., Jordan, S., Napiwotzki, R., et al. 2004, *A&A*, **423**, 1081
- Benvenuto, O. G., & Althaus, L. G. 1999, *MNRAS*, **303**, 30
- Benz, W., Cameron, A. G. W., Press, W. H., & Bowers, R. L. 1990, *ApJ*, **348**, 647
- Bergeron, P., & Liebert, J. 2002, *ApJ*, **566**, 1091
- Bergeron, P., Wesemael, F., Liebert, J., & Fontaine, G. 1989, *ApJ*, **345**, L91
- Bours, M. C. P., Toonen, S., & Nelemans, G. 2013, *A&A*, **552**, A24
- Bragaglia, A., Greggio, L., Renzini, A., & D'Odorico, S. 1990, *ApJ*, **365**, L13
- Branch, D., & Wheeler, J. C. 2017, *Supernova Explosions* (Germany: Springer-Verlag)
- Breedt, E., Steeghs, D., Marsh, T. R., et al. 2017, *MNRAS*, **468**, 2910
- Brown, W. R., Kilic, M., Allende Prieto, C., & Kenyon, S. J. 2010, *ApJ*, **723**, 1072
- Brown, W. R., Kilic, M., Allende Prieto, C., & Kenyon, S. J. 2012, *ApJ*, **744**, 142
- Brown, W. R., Kilic, M., Allende Prieto, C., Gianninas, A., & Kenyon, S. J. 2013, *ApJ*, **769**, 66
- Brown, W. R., Gianninas, A., Kilic, M., Kenyon, S. J., & Allende Prieto, C. 2016a, *ApJ*, **818**, 155
- Brown, W. R., Kilic, M., Kenyon, S. J., & Gianninas, A. 2016b, *ApJ*, **824**, 46
- Christlieb, N., Wisotzki, L., Reimers, D., et al. 2001, *A&A*, **366**, 898
- Dan, M., Rosswog, S., & Brüggen, M. 2009, *J. Phys. Conf. Ser.*, **172**, 012034
- Dan, M., Rosswog, S., Brüggen, M., & Podsiadlowski, P. 2014, *MNRAS*, **438**, 14
- Debes, J. H., Sigurdsson, S., & Woodgate, B. E. 2005, *AJ*, **130**, 1221
- Dekker, H., D'Odorico, S., Kaufer, A., Delabre, B., & Kotzlowski, H. 2000, in *Optical and IR Telescope Instrumentation and Detectors*, eds. M. Iye, & A. F. Moorwood, *SPIE Conf. Ser.*, **4008**, 534
- Dobbie, P. D., Burleigh, M. R., Levan, A. J., et al. 2005, *MNRAS*, **357**, 1049
- Dorman, B., Rood, R. T., & O'Connell, R. W. 1993, *ApJ*, **419**, 596
- D'Souza, M., Motl, P., Tohline, J., & Frank, J. 2006, *ApJ*, **643**, 381
- Faulkner, J., Flannery, B. P., & Warner, B. 1972, *ApJ*, **175**, L79
- Finley, D. S., & Koester, D. 1997, *ApJ*, **489**, L79
- Foss, D., Wade, R. A., & Green, R. F. 1991, *ApJ*, **374**, 281
- Freudling, W., Romaniello, M., Bramich, D. M., et al. 2013, *A&A*, **559**, A96
- Gaia Collaboration (Brown, A. G. A., et al.) 2018, *A&A*, **616**, A1
- Gentile Fusillo, N. P., Tremblay, P.-E., Gänsicke, B. T., et al. 2019, *MNRAS*, **482**, 4570
- Giannichele, N., Bergeron, P., & Dufour, P. 2012, *ApJS*, **199**, 29
- Gianninas, A., Bergeron, P., & Ruiz, M. T. 2011, *ApJ*, **743**, 138
- Giclas, H. L., Burnham, Jr., R., & Thomas, N. G. 1978, *Lowell Obs. Bull.*, **8**, 89
- Giclas, H. L., Burnham, Jr., R., & Thomas, N. G. 1980, *Lowell Obs. Bull.*, **8**, 157
- Grabowski, B., Halenka, J., & Madej, J. 1987, *ApJ*, **313**, 750
- Green, R. F., Schmidt, M., & Liebert, J. 1986, *ApJS*, **61**, 305
- Greenstein, J. L., & Peterson, D. M. 1973, *A&A*, **25**, 29
- Griffin, R. 1973, *MNRAS*, **162**, 243
- Guerrero, J., García-Berro, E., & Isern, J. 2004, *A&A*, **413**, 257
- Hagen, H.-J., Groot, D., Engels, D., & Reimers, D. 1995, *A&AS*, **111**, 195
- Halenka, J., Olchawa, W., Madej, J., & Grabowski, B. 2015, *ApJ*, **808**, 131
- Hamada, T., & Salpeter, E. E. 1961, *ApJ*, **134**, 683
- Heber, U. 2009, *ARA&A*, **47**, 211
- Heber, U. 2016, *PASP*, **128**, 082001
- Heber, U., Napiwotzki, R., & Reid, I. N. 1997a, *A&A*, **323**, 819
- Heber, U., Napiwotzki, R., Lemke, M., & Edelmann, H. 1997b, *A&A*, **324**, L53
- Hillebrandt, W., Kromer, M., Röpke, F. K., & Ruiter, A. J. 2013, *Front. Phys.*, **8**, 116
- Hoard, D. W., Wachter, S., Sturch, L. K., et al. 2007, *AJ*, **134**, 26
- Homeier, D., Koester, D., Hagen, H.-J., et al. 1998, *A&A*, **338**, 563
- Hoyle, F., & Fowler, W. A. 1960, *ApJ*, **132**, 565
- Iben, Jr., I., & Tutukov, A. V. 1984, *ApJS*, **54**, 335
- Iben, Jr., I., & Tutukov, A. V. 1985, *ApJS*, **58**, 661
- Iben, I., Tutukov, A. V., & Yungelson, L. R. 1997, *ApJ*, **475**, 291
- Jordan, S., Koester, D., Vauclair, G., et al. 1998, *A&A*, **330**, 277
- Justham, S., Wolf, C., Podsiadlowski, P., & Han, Z. 2009, *A&A*, **493**, 1081
- Karl, C. 2004, Ph.D. Thesis, Friedrich-Alexander University Erlangen-Nürnberg
- Karl, C. A., Napiwotzki, R., Nelemans, G., et al. 2003, *A&A*, **410**, 663
- Kawka, A., & Vennes, S. 2012, *MNRAS*, **425**, 1394
- Kepler, S. O., Kleinman, S. J., Nitta, A., et al. 2007, *MNRAS*, **375**, 1315
- Kilic, M., Brown, W. R., Allende Prieto, C., et al. 2012, *ApJ*, **751**, 141
- Kilkenny, D., O'Donoghue, D., Koen, C., Stobie, R. S., & Chen, A. 1997, *MNRAS*, **287**, 867
- Koester, D., & Herrero, A. 1988, *ApJ*, **332**, 910
- Koester, D., & Komp, E. 2007, *A&A*, **473**, 239
- Koester, D., Allard, N. F., & Vauclair, G. 1994, *A&A*, **291**, L9
- Koester, D., Dreizler, S., Weidemann, V., & Allard, N. F. 1998, *A&A*, **338**, 612
- Koester, D., Napiwotzki, R., Christlieb, N., et al. 2001, *A&A*, **378**, 556
- Koester, D., Rollenhagen, K., Napiwotzki, R., et al. 2005a, *A&A*, **432**, 1025
- Koester, D., Napiwotzki, R., Voss, B., Homeier, D., & Reimers, D. 2005b, *A&A*, **439**, 317
- Koester, D., Voss, B., Napiwotzki, R., et al. 2009, *A&A*, **505**, 441
- Kulkarni, S. R., & van Kerkwijk, M. H. 2010, *ApJ*, **719**, 1123
- Kupfer, T., Geier, S., Heber, U., et al. 2015, *A&A*, **576**, A44
- Lamontagne, R., Demers, S., Wesemael, F., Fontaine, G., & Irwin, M. J. 2000, *AJ*, **119**, 241
- Landstreet, J. D., Bagnulo, S., Valyavin, G. G., et al. 2012, *A&A*, **545**, A30
- Latour, M., Fontaine, G., Green, E. M., & Brassard, P. 2015, *A&A*, **579**, A39
- Liebert, J., Bergeron, P., Schmidt, G. D., & Saffer, R. A. 1993, *ApJ*, **418**, 426
- Lisker, T., Heber, U., Napiwotzki, R., et al. 2005, *A&A*, **430**, 223
- Livio, M., & Mazzali, P. 2018, *Phys. Rep.*, **736**, 1

- Livne, E. 1990, *ApJ*, 354, L53
- Livne, E., & Glasner, A. 1991, *ApJ*, 370, 272
- Luyten, W. J. 1979, *LHS catalogue. A catalogue of stars with proper motions exceeding 0''5 annually*, 2nd ed. (Minneapolis: University of Minnesota)
- Maoz, D., & Hallakoun, N. 2017, *MNRAS*, 467, 1414
- Maoz, D., Mannucci, F., & Nelemans, G. 2014, *ARA&A*, 52, 107
- Maoz, D., Hallakoun, N., & Badenes, C. 2018, *MNRAS*, 476, 2584
- Marsh, T. R. 1995, *MNRAS*, 275, L1
- Marsh, T. R. 2000, *New Astron. Rev.*, 44, 119
- Marsh, T. R., Dhillon, V. S., & Duck, S. R. 1995, *MNRAS*, 275, 828
- Marsh, T. R., Nelemans, G., & Steeghs, D. 2004, *MNRAS*, 350, 113
- Marsh, T. R., Gänsicke, B. T., Steeghs, D., et al. 2011, *ApJ*, 736, 95
- Maxted, P. F. L., & Marsh, T. R. 1999, *MNRAS*, 307, 122
- Maxted, P. F. L., Marsh, T. R., Moran, C. K. J., & Han, Z. 2000a, *MNRAS*, 314, 334
- Maxted, P. F. L., Marsh, T. R., & Moran, C. K. J. 2000b, *MNRAS*, 319, 305
- Maxted, P. F. L., Burleigh, M. R., Marsh, T. R., & Bannister, N. P. 2002, *MNRAS*, 334, 833
- Maxted, P. F. L., Napiwotzki, R., Dobbie, P. D., & Burleigh, M. R. 2006, *Nature*, 442, 543
- McCook, G. P., & Sion, E. M. 1999, *ApJS*, 121, 1
- Mochkovitch, R., & Livio, M. 1990, *A&A*, 236, 378
- Morales-Rueda, L., Marsh, T. R., Maxted, P. F. L., et al. 2005, *MNRAS*, 359, 648
- Moran, C., Marsh, T. R., & Bragaglia, A. 1997, *MNRAS*, 288, 538
- Napiwotzki, R. 1999, *A&A*, 350, 101
- Napiwotzki, R. 2009, *J. Phys. Conf. Ser.*, 172, 012004
- Napiwotzki, R., Green, P. J., & Saffer, R. A. 1999, *ApJ*, 517, 399
- Napiwotzki, R., Christlieb, N., Drechsel, H., et al. 2001a, *Astron. Nachr.*, 322, 411
- Napiwotzki, R., Edelmann, H., Heber, U., et al. 2001b, *A&A*, 378, L17
- Napiwotzki, R., Koester, D., Nelemans, G., et al. 2002, *A&A*, 386, 957
- Napiwotzki, R., Christlieb, N., Drechsel, H., et al. 2003, *The Messenger*, 112, 25
- Napiwotzki, R., Yungelson, L., Nelemans, G., et al. 2004, in *Spectroscopically and Spatially Resolving the Components of the Close Binary Stars*, eds. R. W. Hilditch, H. Hensberge, & K. Pavlovski, *ASP Conf. Ser.*, 318, 402
- Napiwotzki, R., Karl, C. A., Nelemans, G., et al. 2005, in 14th European Workshop on White Dwarfs, eds. D. Koester, S. Moehler, et al., *ASP Conf. Ser.*, 334, 375
- Napiwotzki, R., Karl, C. A., Nelemans, G., et al. 2007, in 15th European Workshop on White Dwarfs, eds. R. Napiwotzki, M. R. Burleigh, *ASP Conf. Ser.*, 372, 387
- Nelemans, G., & Tauris, T. M. 1998, *A&A*, 335, L85
- Nelemans, G., Yungelson, L. R., Portegies Zwart, S. F., & Verbunt, F. 2001a, *A&A*, 365, 491
- Nelemans, G., Portegies Zwart, S. F., Verbunt, F., & Yungelson, L. R. 2001b, *A&A*, 368, 939
- Nelemans, G., Napiwotzki, R., Karl, C., et al. 2005, *A&A*, 440, 1087
- Nomoto, K., & Iben, I. J. 1985, *ApJ*, 297, 531
- Panei, J. A., Althaus, L. G., Chen, X., & Han, Z. 2007, *MNRAS*, 382, 779
- Parsons, S. G., Hermes, J. J., Marsh, T. R., et al. 2017, *MNRAS*, 471, 976
- Pauli, E.-M., Napiwotzki, R., Altmann, M., et al. 2003, *A&A*, 400, 877
- Pauli, E.-M., Napiwotzki, R., Heber, U., Altmann, M., & Odenkirchen, M. 2006, *A&A*, 447, 173
- Perlmutter, S., Aldering, G., Goldhaber, G., et al. 1999, *ApJ*, 517, 565
- Postnov, K. A., & Yungelson, L. R. 2014, *Liv. Rev. Rel.*, 17, 3
- Pounds, K. A., Allan, D. J., Barber, C., et al. 1993, *MNRAS*, 260, 77
- Press, W. H., Teukolsky, S. A., Vetterling, W. T., & Flannery, B. P. 1992, *Numerical recipes in FORTRAN. The art of scientific computing*, 2nd ed. (Cambridge: University Press)
- Rebassa-Mansergas, A., Parsons, S. G., García-Berro, E., et al. 2017, *MNRAS*, 466, 1575
- Rebassa-Mansergas, A., Toonen, S., Korol, V., & Torres, S. 2019, *MNRAS*, 482, 3656
- Renedo, I., Althaus, L. G., Miller Bertolami, M. M., et al. 2010, *ApJ*, 717, 183
- Renzini, A. 1999, *The Messenger*, 96, 13
- Richter, R., Heber, U., & Napiwotzki, R. 2007, in 15th European Workshop on White Dwarfs, eds. R. Napiwotzki, & M. R. Burleigh, *ASP Conf. Ser.*, 372, 107
- Riess, A. G., Filippenko, A. V., Challis, P., et al. 1998, *AJ*, 116, 1009
- Robinson, E. L., & Shafter, A. W. 1987, *ApJ*, 322, 296
- Röpke, F. K., & Sim, S. A. 2018, *Space Sci. Rev.*, 214, 72
- Ruiz-Lapuente, P. 2014, *New Astron. Rev.*, 62, 15
- Saffer, R. A., Liebert, J., & Olszewski, E. W. 1988, *ApJ*, 334, 947
- Saffer, R. A., Livio, M., & Yungelson, L. R. 1998, *ApJ*, 502, 394
- Sato, Y., Nakasato, N., Tanikawa, A., et al. 2016, *ApJ*, 821, 67
- Scalzo, R., Aldering, G., Antilogus, P., et al. 2014, *MNRAS*, 440, 1498
- Schatzman, E. 1963, in *Star Evolution*, ed. L. Gratton, 389
- Schmidt, G. D., & Smith, P. S. 1994, *ApJ*, 423, L63
- Schmidt, G. D., & Smith, P. S. 1995, *ApJ*, 448, 305
- Shigeyama, T., Nomoto, K., Yamaoka, H., & Thielemann, F.-K. 1992, *ApJ*, 386, L13
- Shipman, H. L., & Mehan, R. G. 1976, *ApJ*, 209, 205
- Sim, S. A., Röpke, F. K., Hillebrandt, W., et al. 2010, *ApJ*, 714, L52
- Skrutskie, M. F., Cutri, R. M., Stiening, R., et al. 2006, *AJ*, 131, 1163
- Solheim, J. E., & Yungelson, L. R. 2005, in 14th European Workshop on White Dwarfs, eds. D. Koester, & S. Moehler, *ASP Conf. Ser.*, 334, 387
- Stroeer, A., Heber, U., Lisker, T., et al. 2007, *A&A*, 462, 269
- Sweigart, A. V. 1994, *ApJ*, 426, 612
- Taubenberger, S. 2017, *The Extremes of Thermonuclear Supernovae* (Heidelberg: Springer), 317
- Tremblay, P.-E., Ludwig, H.-G., Steffen, M., & Freytag, B. 2013, *A&A*, 552, A13
- Truran, J. W., & Cameron, A. G. W. 1971, *Ap&SS*, 14, 179
- Tutukov, A. V., & Yungelson, L. R. 1976, *Astrophysics*, 12, 342
- Tutukov, A. V., & Yungelson, L. R. 1979, *Acta Astron.*, 29, 665
- Tutukov, A. V., & Yungelson, L. R. 1981, *Nauchnye Informatsii*, 49, 3
- Webbink, R. F. 1979, in *IAU Colloq. 53: White Dwarfs and Variable Degenerate Stars*, eds. H. M. van Horn, & V. Weidemann, 426
- Webbink, R. F. 1984, *ApJ*, 277, 355
- Wegg, C., & Phinney, E. S. 2012, *MNRAS*, 426, 427
- Wellhouse, J. W., Hoard, D. W., Howell, S. B., Wachter, S., & Esin, A. A. 2005, *PASP*, 117, 1378
- Werner, K. 1996, *ApJ*, 457, L39
- Wesemael, F., Bergeron, P., Lamontagne, R. L., et al. 1994, *ApJ*, 429, 369
- Wheeler, J. C., & Hansen, C. J. 1971, *Ap&SS*, 11, 373
- Whelan, J., & Iben, Jr., I. 1973, *ApJ*, 186, 1007
- Wiese, W. L., & Kelleher, D. E. 1971, *ApJ*, 166, L59
- Wiese, W. L., Kelleher, D. E., & Paquette, V. 1972, *Phys. Rev. A*, 71, 1132
- Wisotzki, L., Christlieb, N., Bade, N., et al. 2000, *A&A*, 358, 77
- Yungelson, L. R. 2010, *Astron. Lett.*, 36, 780
- Yungelson, L. R., & Kuranov, A. G. 2017, *MNRAS*, 464, 1607
- Zorotovic, M., & Schreiber, M. R. 2017, *MNRAS*, 466, L63

Appendix A: A test of the possible impact of pressure broadening on Balmer lines

The densities in atmospheres of white dwarfs are sufficiently high that pressure shifts of line profiles are a concern. If present, these effects mimic an RV shift. Laboratory experiments by [Wiese & Kelleher \(1971\)](#) and [Wiese et al. \(1972\)](#) measured substantial pressure redshifts for $H\beta$, $H\gamma$, $H\delta$ and to a lesser extent for $H\alpha$. [Shipman & Mehan \(1976\)](#) included the shifts determined in these experiments and solved the radiation transfer for white dwarf atmospheres. The resulting line profiles were analysed following the procedure applied to observed spectra at that time to determine the line centre. This investigation found that effects for $H\alpha$ and $H\beta$ were below the 1 km s^{-1} level. A later analysis by [Grabowski et al. \(1987\)](#) revisited the [Wiese et al. \(1972\)](#) data and carried out a more detailed fit of the measurements with three parameters (plus a correction term). Stellar line profiles were computed using model atmospheres and analysed in a fashion similar to the previous investigation by [Shipman & Mehan \(1976\)](#). The new study by [Grabowski et al. \(1987\)](#) confirmed small pressure shifts for $H\alpha$ exceeding $1\text{--}2 \text{ km s}^{-1}$ only for cool, high gravity ($\log g = 9$) white dwarfs. However, for $H\beta$ the authors find large shifts often in the range $5\text{--}10 \text{ km s}^{-1}$.

A recent study by [Halenka et al. \(2015\)](#) calculated theoretical line profiles using a so-called modified full computer simulation method. This method treats shifts and asymmetries as corrections depending on the local plasma conditions to a simpler first order description of line profiles. The authors compare the new calculations with laboratory data and find improvements to previous attempts. Atmospheric line profiles of $H\alpha$ and $H\beta$ were calculated using the new theoretical calculations. The result is even smaller pressure shifts for $H\alpha$ than reported in [Grabowski et al. \(1987\)](#). The effect does not exceed 1 km s^{-1} even when the measurement is carried out 25 \AA from the line centre. Contrary to that the new study finds an effect for $H\beta$ about twice as large as previously, exceeding 10 km s^{-1} at a distance of 15 \AA . The authors point out that the impact on RV measurements should be very small, if the resolved NLTE core of the lines is measured in high resolution spectra. The Doppler core is formed in low density regions of the atmosphere where the Stark effect is of no importance compared to Doppler broadening.

We carried out an empirical test of the possible impact of $H\beta$ pressure shifts on our RV measurements. We selected a subset of white dwarfs from Table B.1 with clearly visible NLTE core and good spectra, yielding an RV accuracy of 2 km s^{-1} or better. We excluded targets with a gravity below 7.8. Lower gravity white dwarfs have lower density atmospheres, which would result in smaller effects. We selected the first 100 objects fulfilling these criteria from our catalogue with a total of 201 spectra between them (high S/N 100; H100).

Our measurements of the H100 sample are summarised in Table A.1. We first determined the offsets between $H\alpha$ and $H\beta$ measured over the $\pm 15 \text{ \AA}$ interval, i.e. in the same fashion as our original measurements, only that we then included both lines in a simultaneous fit. The result is a very small systematic difference between both lines of -0.8 km s^{-1} . The offset increased to -2.5 km s^{-1} when we increased the fitted interval to $\pm 30 \text{ \AA}$. It can be expected that the largest signal is still delivered by the resolved Doppler broadened NLTE core. We thus convolved the model spectra with a Gaussian of 3 \AA FWHM, which smoothes the core away and tweaked the fit process to give small weights to the Doppler core. This procedure now gives the results from

Table A.1. Systematic shifts measured for the H100 sample.

Measurement	Interval (\AA)	Remark	RV shift (km s^{-1})
$\text{RV}(H\beta)\text{--RV}(H\alpha)$	$\pm 15 \text{ \AA}$		-0.8 ± 0.4
$\text{RV}(H\beta)\text{--RV}(H\alpha)$	$\pm 30 \text{ \AA}$		-2.5 ± 0.4
$\text{RV}(H\beta)\text{--RV}(H\alpha)$	$\pm 30 \text{ \AA}$	Core smoothed	-8.7 ± 0.6
$\text{RV}(H\alpha+H\beta)\text{--RV}_{\text{best}}$	$\pm 30 \text{ \AA}$	Core smoothed	-3.7 ± 0.3

Notes. The 1σ uncertainty of the average is given, calculated using bootstrapping.

measuring the Stark broadened wings only. The offset between $H\beta$ and $H\alpha$ increases to -8.7 km s^{-1} .

Somewhat surprisingly we measure on average smaller RVs for $H\beta$ than for $H\alpha$, i.e. blueshifts not redshifts as predicted by [Halenka et al. \(2015\)](#). However, let us keep in mind that the fit process includes a normalisation of model and observed spectrum. It is well possible that this will cancel out, or maybe, even overcompensate line asymmetries. [Halenka et al. \(2015\)](#) carried out a normalisation of their model spectra, but used the true continuum for this exercise. The FITSB2 normalisation process, as applied for our measurements, restricts itself to the fitted region. An asymmetry in the outer wings of the line, if present, will thus result in a tilt.

A detailed investigation is beyond the scope of this article. Our main interest here is an estimate of possible systematic offsets of our RVs. The small RV offset between $H\alpha$ and $H\beta$ measurements for our H100 sample done the standard way over the $\pm 15 \text{ \AA}$ interval gives us confidence that the systematic RV errors for white dwarfs with well developed NLTE cores is not larger than 1 km s^{-1} . Note also the good agreement between our RVs measured from Balmer lines and the Ca K line (Fig. 7).

We used the best guess RVs (RV_{best}) from Table B.1 as reference point to get an estimate of systematic offsets for RVs measured using the $\pm 30 \text{ \AA}$ interval. We fitted RVs of our H100 sample over $\pm 30 \text{ \AA}$, combining $H\alpha$ and $H\beta$, the NLTE core smoothed away. The average difference to RV_{best} is -3.7 km s^{-1} .

We actually do not know RV_{best} for DA targets with weak NLTE cores, for which we needed to use a wider fit interval. However, we made an attempt to measure the differences between $H\alpha$ and $H\beta$ RVs. Uncertainties are quite substantial due to the weak features of these spectra. These measurements also produced a few outliers, a tendency which is much reduced if both Balmer lines are combined. This is the main reason we included $H\beta$ for our RV measurements in the first place. To avoid spurious results we excluded spectra with an uncertainty of the RV difference exceeding 15 km s^{-1} . The average of the remaining 31 measurements has an RV offset of $-14.6 \pm 2.6 \text{ km s}^{-1}$. This is larger than what we measured for our H100 sample with smoothed NLTE core. It is plausible that the generally weaker features of these stars increase the impact of line asymmetries or other systematics. Assuming that the pattern observed for the H100 sample holds, we estimate that the systematic error for the simultaneous fit of $H\alpha$ and $H\beta$ amounts to about -7 km s^{-1} .

In summary we estimate that systematic offsets of the DAs with prominent NLTE cores (the vast majority) should not exceed 1 km s^{-1} , for targets with weak Doppler cores a systematic offset of about 7 km s^{-1} is possible. These are small enough that they will have no impact on the *relative* RV measurements at different epochs, but need to be considered for *absolute* RVs.

Appendix B: Radial velocity measurements for all DA white dwarfs

Table B.1 lists all RV measurements of the DA white dwarfs in the SPY sample.

Column 1: Designation. “WD” indicates that this source was selected from the [McCook & Sion \(1999\)](#) version of the WD catalogue. Other designations indicate that other sources were used (see text).

Column 2: Julian date. The dates are for mid-exposure and corrected to heliocentric values.

Column 3: Individual heliocentric RV measurements for the epochs. If photospheric Ca II lines were present, the Ca K lines were included in the measurement. Observations done under poor conditions (usually repeated afterwards) are included in this table. Errors are often large due to poor signal to noise levels, but could carry useful phase information.

Column 4: Wavelengths range used for the RV measurements, shifted according to the measured RV. An empty entry indicates the standard $\pm 15 \text{ \AA}$ interval. Larger values were used, when a sharp line core was missing (see text). Sometimes an asymmetric range was chosen to avoid flaws in the spectra.

Column 5: Weighted average of the RV measurements. The error is computed including the estimate for instrumental

systematics calculated from the telluric lines and comparison between Ca and H lines when present.

Column 6: χ^2 values computed for the null hypothesis that RV is constant. Again, our estimates for the systematic errors are included.

Column 7: The next column gives the probability p that χ^2 has a value as high as the measured one or higher for an RV constant star. The smaller the values the higher the confidence that the star is RV variable.

Column 8: A binary is assumed for probability $\log p < -4$ and marked as DD in this column. Double-lined systems not exceeding our RV variation threshold, but identified by visual inspection are marked dd.

Column 9: Comments and observations. Abbreviations:

- SB2: Double-lined DD.
- G&L: Model spectrum modified using one or more Gaussians and Lorentzians (see text).
- polyn.: Model spectrum modified using a low order polynomial.
- v_{rot} : Rotation included in fit. That does not necessary indicate that the star is rotating. The aim was to achieve a good match of the observed profiles for fitting RVs without considerations of the physical soundness.
- +Ca K: Photospheric Ca II present and included in fit.

Table B.1. RV measurements for the SPY DA white dwarfs.

Object	HJD	RV	$\Delta\lambda$	\overline{RV}	χ^2	$\log p$	comments
	–2 400 000	(km s^{-1})	(\AA)	(km s^{-1})			
WD2359–434	51739.7790	49.6 ± 1.4		48.7 ± 1.1	0.40	–0.28	polyn., G&L, v_{rot}
	51743.8041	47.7 ± 1.5					
WD2359–324	51740.7447	94.7 ± 5.6		81.6 ± 2.4	4.36	–0.95	
	51742.8050	72.6 ± 6.8					
	52799.9168	79.9 ± 2.7					
WD0000–186	51803.7127	25.3 ± 1.7		24.2 ± 1.3	0.36	–0.26	
	51804.6533	23.3 ± 1.7					
HS0002+1635	52610.5530	18.2 ± 2.1		16.4 ± 1.4	0.63	–0.37	
	52889.7085	15.2 ± 1.7					
⋮	⋮	⋮		⋮	⋮	⋮	

Notes. Full table available at CDS.

Appendix C: Fundamental parameters

Table C.1. References and explanations for Table C.2.

Ambiguous	Koester et al. (2009) reported a cool and a hot solution. The solution yielding the smallest χ^2 is included.
BL02	Bergeron & Liebert (2002)
GBD12, phot	Giannichele et al. (2012), T_{eff} and $\log g$ derived from photometric spectral energy distribution and trigonometric parallax.
GBR11	Gianninas et al. (2011), fit of Balmer lines
KNV05	Koester et al. (2005b), helium-rich DABZ
KV12	Kawka & Vennes (2012), fit of Balmer lines
LBSS93	Liebert et al. (1993), binary of magnetic and non-magnetic WD
Magnetic	magnetic DAs, Zeeman splitting of the line cores. See text for details on the fit procedure.
New	white dwarf not included in the Koester et al. (2009) analysis. Analysed using the same model grid.
New/NLTE	hot DAO white dwarfs, analysed using the grid of NLTE model atmospheres described in Napiwotzki (1999).
Primary	Parameters of the primary from a simultaneous fit of primary and secondary. See text.
WB94	Wesemael et al. (1994), fit of primary and secondary parameters using lines and spectral energy distribution
HNLE97	Heber et al. (1997b): genuine DAB, helium line profile variations
K09	Koester et al. (2009): visual double
FK97	Finley & Koester (1997): visual double
J98	Jordan et al. (1998): visual double

Table C.2 lists the fundamental parameters surface temperature and gravity adopted for our targets. Most of these values are taken from Koester et al. (2009) who determined temperatures and gravities of sample stars by fitting the Balmer lines of the SPY spectra. The table lists effective temperatures and gravities, with the 3D atmosphere corrections of Tremblay et al. (2013) for DAs with a convective envelope (mixing length parameter $ML2/\alpha = 0.6$). White dwarf masses were estimated from interpolation in the white dwarf cooling tracks of Panei et al. (2007), Renedo et al. (2010) and Althaus et al. (2005).

Koester et al. (2009) did not derive parameters for some DAs of the sample for various reasons, including a few cases of objects overlooked. For some other cases we decided to replace the values as discussed below. Notes and references have been included in Col. 5 of Table C.2 and explained in Table C.1, whenever values different from those given by Koester et al. (2009) were included.

Double-lined binaries: Light of both components is seen in the spectra of double-lined binaries. A deconvolution of both components was attempted using FITSB2 and the same DA model grid as used by Koester et al. (2009). An iterative procedure was carried out starting with a simple by-eye estimate of the RVs in the spectra, followed by a fit of temperatures and gravities of both components. These were then used for improved estimates of RVs from the cores of $H\alpha$ and $H\beta$ as described in Sect. 3.2. The latter two steps were repeated until the iteration came to a standstill. The relative contributions of both

Table C.2. Gaia DR2 IDs, effective temperatures, gravities and masses for the SPY DA white dwarfs.

Object	Gaia DR2 ID	T_{eff} (K)	$\log g$ (cm s^{-1})	M (M_{\odot})	References/ remarks
WD2359–434	4994877094997259264	8253	8.01	0.604	Magnetic
WD2359–324	2313582750735435776	22478	7.74	0.514	
WD0000–186	2414099622710507904	15264	7.85	0.535	
HS0002+1635	2772855182928578560	25878	7.86	0.568	
WD0005–163	2416481783371550976	11860	7.60	0.435	Ambiguous
WD0011+000	2545505281002947200	9423	7.77	0.492	
WD0013–241	2336189396997071616	18529	7.90	0.568	
WD0016–258	2323704339384503040	10874	7.80	0.507	
WD0016–220	2361264618662161920	13622	7.75	0.496	
WD0017+061	2747611250653031040	28149	7.75	0.526	
⋮	⋮	⋮	⋮	⋮	

Notes. Full table available at CDS.

components were determined using mass-radius relations from the cooling tracks above. The fundamental parameters listed in Tables C.2 and B.1 correspond to the primary (i.e. the brighter component).

The fundamental parameters listed for the primaries are tentative and should be replaced by results from full orbital solutions once these are available. They were derived for the purpose of assessing the status of the primary as low-mass He core or C/O core white dwarf.

Magnetic white dwarfs: Magnetic white dwarfs included in this study have fields strong enough to induce a detectable Zeeman splitting in the cores of the Balmer lines, but the lines do not show distortion beyond that. A detailed analysis of the field structure was beyond the scope of this article and we adopted a crude approximation to derive fundamental parameters. Model spectra from standard model atmospheres were co-added after applying shifts. The π component was assumed unshifted and a symmetric shift was applied to the two σ components. Geometric effects were only taken into account by adjusting the relative strength of the π and σ components. This approach is oversimplistic and ignores subtle effects of radiation transfer and field geometry, but our main aim was to get still useful estimates of fundamental parameters, even if of somewhat limited accuracy.

Grids were constructed for a range of splits. For a given magnetic white dwarf best fit values of temperature and gravity were derived for each grid. Values corresponding to the Zeeman split yielding the smallest value of χ^2 were adopted. While we deem the accuracy of the fundamental parameters sufficient to assess the nature (high or low mass) of the white dwarfs, investigators with a specific interest in these stars are advised to carry out a more sophisticated analysis.

Cool white dwarfs: It has been known for some time that the accuracy of surface gravity measurements from Balmer lines alone decreases considerably for white dwarfs at temperatures below ≈ 6500 K (see, e.g., Fig. 2 of Kawka & Vennes 2012). Higher accuracy can be achieved, if parallax measurements are available. We replaced spectroscopy-only values by the parallax based photometric values of Giannichele et al. (2012), if available. Spectroscopic-only fundamental parameters were not included when assessing the number of single and binary white dwarfs in the mass ranges in Table 3 and the discussion (Sect. 5). This is indicated by the lack of a mass entry in Table C.2. All white dwarfs are included in the numbers for the full sample.